Analyzing the chemical composition, morphology and size of ice-nucleating particles by coupling a scanning electron microscope to an offline diffusion chamber

Lisa Schneider[1], Jann Schrod[2], Daniel Weber[2,a], Heinz Bingemer[2], Konrad Kandler[1], Joachim Curtius[2], Martin Ebert[1]

[1]Institute of Applied Geoscience, Technical University of Darmstadt, Darmstadt, 64287, Germany
[2]Institute for Atmospheric and Environmental Sciences, Goethe University Frankfurt, Frankfurt am Main, 60438, Germany
[a]now at: Federal Waterways Engineering and Research Institute, Karlsruhe, 76187, Germany

Correspondence to: ~~Lisa Schneider (schneider@geo.tu-darmstadt.de);~~ Martin Ebert (mebert@geo.tu-darmstadt.de)

Abstract. To understand and predict the formation of clouds and ~~rain~~ precipitation and their influence on our climate, it is crucial to know the characteristics and abundance of ice-nucleating particles (INPs) in the atmosphere. As the ice-nucleating efficiency is a result of individual particle properties, a detailed knowledge on these properties is essential. Here, ~~we present~~ an offline method for the comprehensive single particle analysis of ambient INPs that benefits from the combination of two instruments already used for ice nucleation measurements is presented,~~,~~ focusing on the methodological description of the coupling, whereby strengths and weaknesses of the method are discussed.

~~-~~First, the aerosol is sampled on silicon wafers. INPs are then activated at different temperature and humidity conditions in the deposition nucleation and condensation freezing mode using a static diffusion chamber. ~~Activated INPs~~The positions of grown ice crystals are ~~located~~ defined by~~in~~ a coordinate system, which allows for~~-~~ recovery and detailed analysis of the individual INPs ~~particles causing the nucleation in~~ by a scanning electron microscope. Based on their ~~Here, the size, chemistry and morphology of the particles are identified.~~ physico-chemical properties (chemistry and morphology) ~~Finally,~~ the INPs ~~are~~ can be classified into categories ~~based on their measured properties~~. In combination with the size information, ~~As a result,~~ a size~~-~~ resolved ~~spectrum~~ distribution of the INP classes can be determined. Such results ~~are~~are useful for evaluating INP type-specific parametrizations, e.g., for use in atmospheric modeling, and in closure studies.

A case study from the high-altitude research station Jungfraujoch, Switzerland shows that the targeted INP analysis as obtained by this method is able to identify the main INP classes in reliable proportions. ~~The performance of this coupling method is investigated in a case study on samples from the high-altitude field side Jungfraujoch (JFJ), Switzerland. 200 individual INPs from 14 samples obtained during a 5-week period were classified.~~ Most of the deposition nucleation / condensation freezing mode INPs ~~from Jungfraujoch,~~ activated at -30 °C, ~~were of~~ indicated a geogenic mineral origin (mainly aluminosilicates / Al-rich particles, but also carbonates and silica). ~~Further~~Other major contribution~~s~~rs were ~~from~~

carbon-richcarbonaceous particles, consisting of both smaller soot particles and larger biological particles, and mixed particles (mostly Al/C mixed particles). irregular shape The INPs and had projected area diameters in the rangeranging from 300 nm to 35 µm, with a distinct maximum at 1 - 2 µm. Mineral particles were present throughout the entire size range, while mixed particles A major contribution of mineral particles, mainly aluminosilicates / Al-rich particles, but also carbonates and silica, was identified for the entire INP size spectrum at -30°C. Further contributions were from carbon-rich particles, consisting of both smaller soot particles and larger biological particles. Mixed particles, here mostly particles rich in Al and C, were identified in higher abundances primarily betweenat sizes of 3 µm and above and 9 µm. Minor contributions were seen from sulfates and metal oxides, with the latter ones found with an increased proportion in the size range below 500 nm. During a Saharan dust event, a significant increase of mineral particles in the INP composition was detected.

Such results are useful for evaluating INP-type-specific parametrizations, e.g., for use in atmospheric modeling, and in closure studies.

1 Introduction

Ice-nucleating particles (INPs) have a significant impact on climate and weather. They influence cloud formation and thus have an effect on cloud structure, extent and lifetime, as well as on radiation and precipitation properties (e.g. Kanji et al., 2017, and references therein).

Ice formation in the atmosphere can happen be initiated via several mechanisms depending on ambient conditions. At temperatures below approximately -38 °C, supercooled solution droplets may freeze spontaneously without a crystallization nucleus (homogeneous freezing). To start ice formation at warmer temperatures (T > -38 °C), the energy barrier for nucleation has to be reduced. This can be accomplished by the presence of an INP. Conventionally, four mechanisms are distinguished for heterogeneous freezing processes: (1) deposition nucleation, (2) condensation freezing, (3) contact freezing and (4) immersion freezing. Detailed information on ice nucleation terminology can be found e.g., in Vali et al. (2015) and Kanji et al. (2017). The main focus of recent INP-related research has been on the temperature range determined by heterogeneous nucleation which occurs in mixed phase clouds. But INPs may also be important at lower temperature ranges in the cirrus cloud regime, that is often solely associated with homogeneous nucleation (e.g., Murray & Liu, 2022).

Only a small fraction of the total aerosol can act as INPs and their concentrations can show variations of several orders of magnitude in space and time (DeMott et al., 2010; Kanji et al., 2017). In addition to the prevailing environmental conditions (e.g., i.e., temperature / and humidity), the potential for an INP to become activated is dependent upon various factors, including individual particle properties and its history within the atmosphere. With regard to particle properties, particularly (surface characteristics such as imperfections (e.g., cracks, fissures, edges) (Kiselev et al., 2016) and / or, chemical composition and specific chemical properties (e.g., functional groups like hydrogen bridging (Kanji et al., 2008), crystal structure, coating (Kanji et al., 2008), etc.) as well as its atmospheric processing including potential agglomeration or pre-

activation (Marcolli, 2017)~~can affect the ice-forming capabilities of a particle~~. The~~se~~ promoting sites on the surface of an INP are termed active sites. As particle size increases, the number of active sites also tends to increase. So typically, the larger an atmospheric particle is, the more likely it is to act as an INP (~~e.g.,~~ Archuleta et al., 2005; ~~Hoose & Möhler, 2012~~Welti et al., 2009). ~~Moreover, the particle's history in the atmosphere and potential modifications (coating, agglomeration, pre-activation (Abdelmonem et al., 2020)) may be also important factors for activating it. Given the multitude of factors that influence INP activation, it is not surprising that their concentrations show variations of several orders of magnitude in space and time (e.g., Kanji et al., 2017; DeMott et al., 2010). For instance, with a decrease in temperature by a few degrees Celsius, the INP concentration can increase by an order of magnitude or more (e.g., Petters & Wright, 2015; Kanji et al., 2017).~~

Ice-forming activity has been verified for many atmospheric particle classes. Mineral dust, which is emitted from arid and semi-arid regions and is globally distributed in the atmosphere (Perry et al., 1997; Ansmann et al., 2003; ~~e.g.,~~ Schepanski et al., 2018~~; Perry et al., 1997; Ansmann et al., 2003~~), is ~~an important factor in atmospheric heterogeneous ice formation~~ a good INP at temperatures below -15 °C (Hoose & Möhler, 2012). The composition of mineral dust is highly variable depending on the source region (Scheuvens & Kandler, 2014). Furthermore, soil dust (mineral dust which is often mixed internally with organic components) from agricultural regions is regarded to be a source of INPs (~~e.g.,~~ O'Sullivan et al., 2014). Metal oxides can be components of mineral dust from natural sources and are also emitted by anthropogenic sources. Their efficiency to activate as INPs depends on the type of metallic ~~particle~~ cation as well as on the oxidation state (~~Kanji et al., 2017~~Archuleta et al., 2005; Yakobi-Hancock et al., 2013). At temperatures warmer than -15 °C, mainly biological INPs are ice active (~~e.g., Kanji et al., 2017;~~ Després et al., 2012, and references therein). These include primary particles such as bacteria, fungal spore, pollen and plant debris, as well as some biological macromolecules (~~e.g.,~~ Pummer et al., 2012). Particles from biomass burning and fossil fuel combustion are considered as another particle class relevant for ice formation. This includes soot (mostly a mixture of black carbon with organic carbon) as a product of incomplete combustion as well as fly ash from the non-combustible components. However, the contribution of soot to atmospheric ice formation is still subject of discussion, e.g., Cozic et al. (2008) and Kupiszewski et al. (2016) found opposing results at the same location. Besides the continental sources, the oceans also serve as a source for atmospheric INPs. In addition to sea salt, sea spray aerosol also contains increased amounts of marine organic material from the sea surface microlayer, which is considered to have significant ice-nucleating properties (Wilson et al., 2015).

A detailed overview of all atmospherically relevant INPs is given ~~e.g.,~~ by Kanji et al. (2017) and Burrows et al. (2022).

~~Methodically, there are three main approaches to investigate the relevant INP species, their concentrations and role in cloud formation.~~

~~(1) In laboratory experiments, selected test aerosols can be activated under controlled conditions. Such experiments can provide important information about the ice-forming properties of individual aerosol types and defined mixtures (e.g., Hoose & Möhler, 2012; Hiranuma et al., 2015; DeMott et al., 2018; Hiranuma et al., 2019).~~

~~(2) INPs can be analyzed in field experiments to gain information about their local concentration and to identify particle types and sizes which initiate the ice nucleation process in the atmosphere depending on temperature range, geographic location, etc. (e.g., Wex et al., 2019; Schrod et al., 2020b; Brasseur et al., 2022; Lacher et al., 2024).~~

~~(3) Model simulations are of great importance to assess the impact of aerosol on cloud microphysics, estimating cloud-aerosol feedbacks and predicting cloud radiation and precipitation processes. For these modelling tasks it is essential to improve the representation of INPs and their correlation to type-specific aerosol particles in the simulations. The concentration and main chemical composition of aerosol for a given time and location in the troposphere are meanwhile available from models. To relate the main aerosol types to their ice nucleation ability it is therefore necessary to identify the composition of those particles that nucleate ice. Burrows et al. (2022) identified a key need for a closure study that combines size-resolved aerosol composition measurements, particle class dependent INP parametrizations and INP measurements. In order to evaluate the results of such a closure study in the most comprehensive way, the INP measurements ideally contain, in addition to the INP concentration, information on the size and chemistry of the ice-forming particles. However, gaining this desired set of experimental parameters from field measurements is challenging.~~

Although there is a variety of methods to determine the INP concentration in the laboratory (Hoose & Möhler, 2012; Hiranuma et al., 2015; DeMott et al., 2018; Hiranuma et al., 2019) and in the field (Wex et al., 2019; Schrod et al., 2020b; Brasseur et al., 2022; Lacher et al., 2024), only a few of them are simultaneously able to report on the chemical characteristics of individual ice-nucleating particles ~~(Cziczo et al., 2017)~~.

hat formatiert: Englisch (Vereinigte Staaten)

~~In terms of interpreting the results from ice-forming particle experiments, a distinction has to be made between INPs and ice residuals (IRs). As defined by Cziczo et al. (2017), INPs are those particles that are activated under defined conditions after the collection of the total aerosol, while IRs are those particles remaining after the evaporation of atmospherically formed ice crystals in clouds.~~ Most analytical methods for the chemical characterization of ambient ice nuclei are based on the principle of first separating the ice nuclei or ice particles from the total atmospheric aerosol using different approaches. ~~To analyze IRs, I~~ice crystals can be separated directly from clouds by using specialized inlets (~~e.g.,~~ Schwarzenböck et al., 2000; Mertes et al., 2007; Schenk et al., 2014; Kupiszewski et al., 2015~~; Schenk et al., 2014~~). In this case, the particles are heated after separation so that the water evaporates and ice residuals (IR) remain.~~Analyzing IRs provides information on atmospherically activated particles, but at the same time bears the risk of collecting non-ice-forming particles that have been attached to the ice crystals (Cziczo et al., 2017). By activation of the sampled non-activated total aerosol~~ In another approach, the particles are activated under defined conditions in ~~within~~ an online reaction chamber (e.g., Rogers, 1988) ~~INPs can be identified~~after the collection of the total aerosol. To analyze the~~se INPs~~ activated particles, it is necessary to separate the ice crystals from droplets and evaporate the ice by one of the ~~previously described~~specialized inlet systems or a droplet evaporation zone. ~~In~~

~~both cases, whether direct sampling from clouds (IR) or subsequent activation (INP), the particles' appearances may have undergone alterations due to ice evaporation processes, which could have resulted in differences between the initially activated particle and those analyzed subsequently.~~

In a second step, the separated INPs/IRs are then either analyzed in the air stream or separated and transferred to an offline analysis. To our knowledge, the only online experiment that has been used to determine all particle groups relevant to ice nucleation simultaneously is single particle mass spectrometry (SPMS) (Thomson et al., 2000; ~~e.g.,~~ Kamphus et al., 2010; Brands et al., 2011~~; Thomson et al., 2000~~). In general, online methods allow a real-time analysis with the potential of high ~~temporal~~ time resolution but may have problems at low INP concentrations. However, several studies have reliably demonstrated the coupling between a separation technique and SPMS in a field setting (~~e.g.,~~ Cozic et al., 2008; Pratt et al., 2009; Cziczo et al., 2009; Kamphus et al., 2010; Cziczo et al., 2013; Schmidt et al. 2017; Lacher et al. 2021). ~~Most measurements still rely on indirect information of the supporting aerosol data.~~

Electron microscopy (EM), as an offline method, offers an alternative approach to study the chemical composition of INPs/IRs. For single particle analysis by EM, INPs or IRs are collected on substrates ~~by one of the separation techniques described above~~after evaporating the ice phase.~~.~~ Single particle analysis can be ~~done~~performed automated for large data sets or manually with operator control~~led~~ (Eriksen Hammer et al., 2019). Even though the method cannot provide high temporal resolution measurements due to longer sampling times, it ~~is able to obtain~~ can provide detailed information on morphology ~~and mixing state~~ in addition to chemistry and size of individual INPs and IRs (~~e.g.,~~ Mertes et al., 2007; Prenni et al., 2009; Cziczo et al., 2009; Ebert et al., 2011; Cziczo et al., 2013; Worringen et al. 2015; Eriksen Hammer et al., 2018). ~~For single particle analysis by EM, INPs or IRs are collected on substrates by one of the separation techniques described above. Single particle analysis can be done automated for large data sets or operator controlled (Eriksen Hammer et al., 2019).~~

These methods typically analyze large numbers of INPs/IRs. However, the major challenge of all these methods is that due to the extremely low number of INPs within a sampled air volume compared to the much higher number of non-INP particles (ratio ~ $1/10^4$ – $1/10^6$), the separation must be carried out with a very high accuracy. Even with an accuracy of 99.9 % for INP separation, this would mean that for every correctly separated INP 1000 non-INP particles would be separated incorrectly, when an INP to total aerosol ratio of $1/10^6$ is assumed. In this way, no conclusions about the chemistry of the INP would be possible at all, since there is no way to distinguish particles that have been falsely separated as INP from real INP afterwards. There is also the risk that additional artifacts can be introduced into the INP fraction during the multi-step process. This problem is partially illustrated in the comparison of the chemical analysis of the INP/IR fraction by three different methods in Worringen et al. (2015).

This paper describes an offline method for measuring atmospheric INP concentration in combination with a subsequent characterization of the activated INPs. The recently established method couples the ice nucleation counter FRankfurt Ice nucleation Deposition freezinG Experiment (FRIDGE) to a scanning electron microscope (SEM~~) (a schematic overview is~~

~~shown in Fig. 1)~~). With this method, individual particles can be specifically analyzed, of which it is known that the ice formation has taken place on the substrate exactly at their position. ~~In this method, particles collected from ambient aerosol onto substrates are analyzed with respect to their ice nucleation ability at various combinations of activation temperature and supersaturation with respect to ice, yielding the INP concentration. The activated INPs can subsequently be characterized by SEM with regard to their properties influencing the formation of ice (chemistry, morphology and size). According to the definition by Cziczo et al. (2017) the analyzed particles are referred to as INPs, even if we characterize them by SEM after activation and evaporation in FRIDGE.~~ ~~While t~~The FRIDGE-SEM-coupling technique has been used for several campaigns in recent years, providing valuable results (Schrod et al., 2017; Schrod et al., 2020b; Weber, 2019; He et al., 2023). Details of the FRIDGE method were described by Schrod et al. (2016).~~:~~

~~T~~the present publication expands significantly on these studies by ~~details~~ing the technical procedure to gain reliable information on physico-chemical properties of INPs by SEM, which were previously activated in FRIDGE. The first part of the paper presents a detailed description of the FRIDGE-SEM coupling~~method~~ ~~,~~ highlighting the strengths and discussing the weaknesses - ~~while the second part discusses~~ followed by the results of a case study ~~done~~from the ~~at the~~ h~~H~~igh-a~~A~~ltitude r~~R~~esearch s~~S~~tation Jungfraujoch (JFJ), Switzerland in 2017.

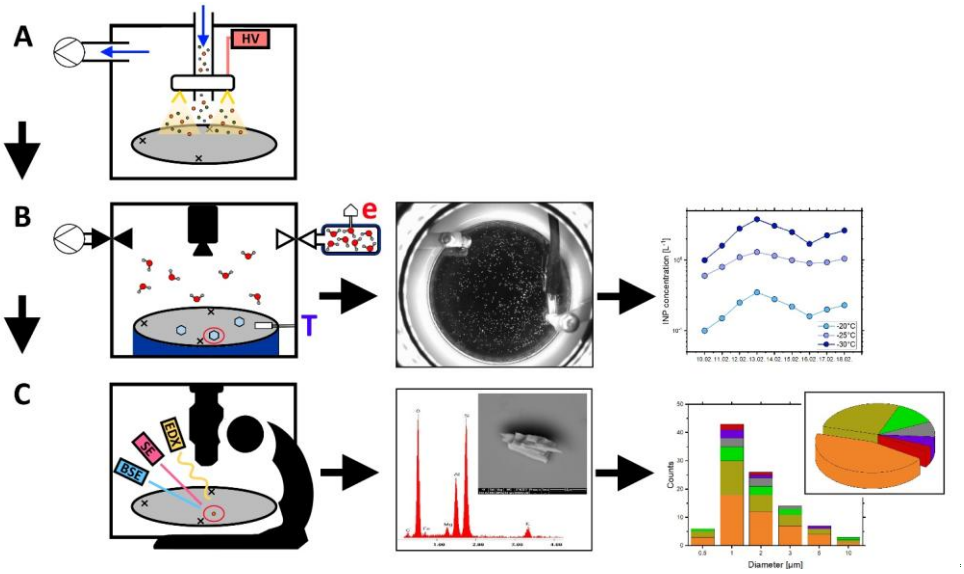

Figure 1: Schematic for the coupled INP analysis. (A) EAC: The aerosol (colored dots) is pumped through the sampling unit in the direction of the blue arrows. By applying high voltage (HV), gold filaments (yellow) arranged in a ring generate an electrostatic field (light yellow triangles). The charged particles are deposited on the silicon substrate (gray). (B) FRIDGE: Diffusion chamber setup with silicon substrate (gray) placed on the cold stage (dark blue) equipped with a temperature sensor (T). The water vapor pressure (e) in the water vapor source (top right) is measured with a pressure sensor. A vacuum pump (top left) is used to evacuate the reaction chamber before the measurement starts. Starting a measurement, the valve to the water vapor source is opened, the diffusion chamber gets flooded with water vapor (red/grey molecules) and ice crystals (light blue) start to grow on the substrate. A camera (top center) monitors the ice growth and records images (see second picture). This can be used to calculate an INP number concentration for different temperature and humidity settings (third picture). (C) SEM: Silicon substrate (grey) with the three engraved crosses defining the coordinate system, placed in the scanning electron microscope (black schematic) equipped with several detectors (solid state detector (blue), Everhart-Thornley detector (red) and energy dispersive x-ray detector (yellow)). Each individual INP which induced ice crystal growth in FRIDGE (particle circled in red) is chemically and morphologically analyzed. The result is a secondary- and backscattered-electron particle image and an elemental spectrum (second picture). As a final result, all the individual particle information is combined in a bulk chemical composition and a chemically resolved size distribution (third picture).

While the FRIDGE-SEM-coupling technique has been used for several campaigns in recent years, providing valuable results (Schrod et al., 2017; Schrod et al., 2020b; Weber, 2019; He et al., 2023), the present publication details the technical procedure. The first part of the paper presents a detailed description of the method, while the second part discusses the results of a case study done at the High-Altitude Research Station Jungfraujoch (JFJ), Switzerland in 2017.

Formatiert: Standard

2 Methodology: Coupling a scanning electron microscope to an ice nucleus counter

The here presented offline coupling procedure (Fig. 1) combines the advantage of two devices which are already used for several years in the field of INP/IR research. Particles can be collected from ambient aerosol onto substrates by electrostatic precipitation (Fig. 1A). The sampled aerosol is then analyzed with respect to its ice nucleation ability at various combinations of activation temperature and supersaturation with respect to ice, yielding the INP concentration (Fig. 1B). The activated INPs can subsequently be characterized by SEM to gain information on their chemistry, morphology and size (Fig. 1C). Based on the definition by Cziczo et al. (2017) we refer to the identified particles as INP, as they were activated under defined conditions after the collection of the total aerosol and not sampled as ice crystals. **Therefore, we are able to investigate truly activated particles in contrast to methods analyzing IRs, which face challenges in order to distinguish between IRs and scavenged particles.** However, some of the INPs analyzed with SEM may have undergone changes due to the measurement procedure in FRIDGE, but we assume that these changes are of minor importance for the main INP classes that we can analyze with this method (see Sect. 2.6).

hat formatiert: Schriftfarbe: Automatisch

215

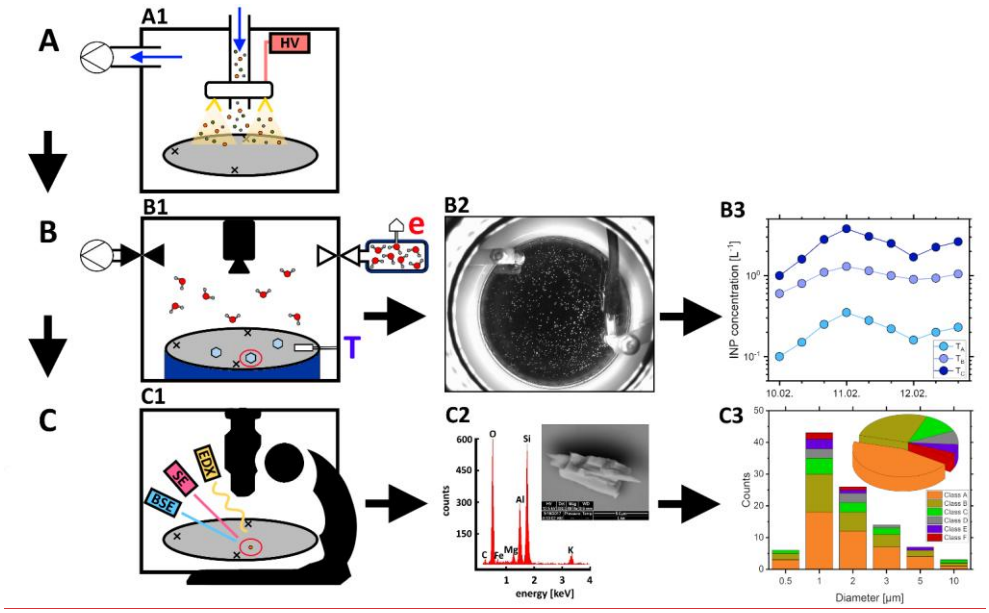
A
A1
HV
B
B1
e
T
B2
B3
INP concentration [L⁻¹]
10.02.
11.02.
12.02.
C
C1
SE
EDX
BSE
C2
counts
energy [keV]
C3
Counts
Diameter [µm]

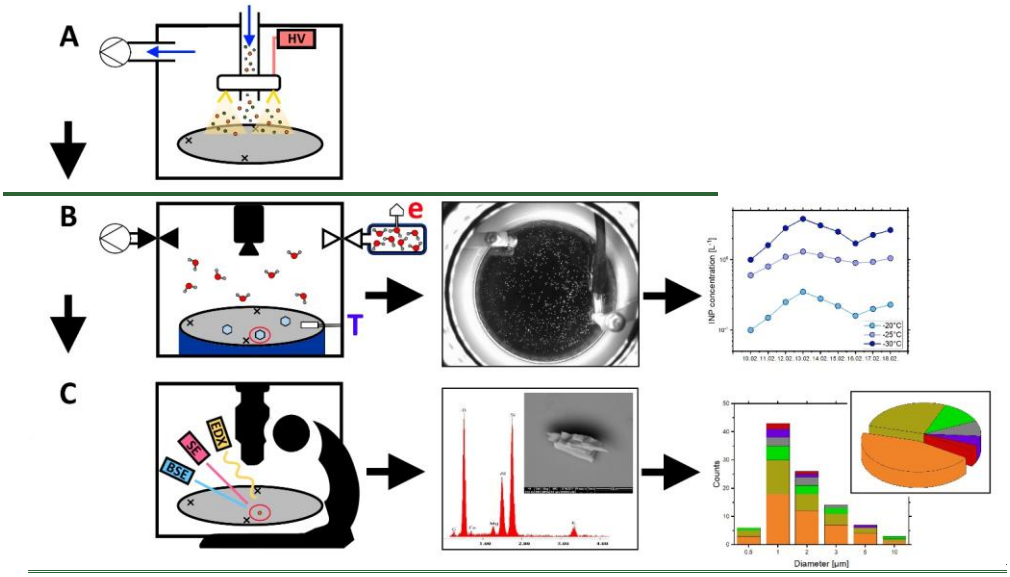

Figure 1: Schematic for the coupled INP analysis. (A) Electrostatic Aerosol Collector (EAC): The aerosol (colored ~~dots~~particles) is pumped through the sampling unit in the direction of the blue arrows. By applying a high voltage (HV), gold filaments (yellow) arranged in a ring generate an electrostatic field (light yellow triangles). The charged particles are deposited on the silicon substrate (gray). (B) FRIDGE: Diffusion chamber setup (B1) with silicon substrate (gray) placed on the cold stage (dark blue) equipped with a temperature sensor (T). The water vapor pressure (e) in the water vapor source (top right) is measured with a pressure sensor. A vacuum pump (top left) is used to evacuate the reaction chamber before the measurement starts. Starting a measurement, the valve to the water vapor source is opened, the diffusion chamber gets flooded with water vapor (red/grey molecules) and ice crystals (light blue) start to grow on the substrate. A camera (top center) monitors the ice growth and records images (~~see second picture~~B2). This can be used to calculate an INP number concentration for different temperature and humidity settings (~~third picture~~B3). (C) SEM: Silicon substrate (grey) with the three engraved crosses defining the coordinate system, placed in the scanning electron microscope (black schematic) equipped with several detectors (solid state detector (blue), Everhart-Thornley detector (red) and energy dispersive x-ray detector (yellow)) (C1). Each individual INP which induced ice crystal growth in FRIDGE (particle circled in red) is chemically and morphologically analyzed. The result is a secondary- and backscattered-electron particle image and an elemental spectrum (~~second picture~~C2). As a final result, all the individual particle information is combined in a bulk chemical composition and a chemically ~~-~~resolved size distribution (~~third picture~~C3).

Formatiert: Standard

Formatiert: Zeilenabstand: 1,5 Zeilen

2.1 Sample substrates

A silicon disk with a diameter of 45 mm serves as the sample substrate, on which the aerosol particles are deposited by electrostatic precipitation (see Sect. 2.2). The semi-conductive substrate is made from commercially available silicon wafers,

which are widely used as basis for microchips in electronic devices. The pure crystalline silicon surface is highly inefficient for ice-nucleation, which prevents ~~from~~ random icing on the wafer, that would induce an artificial background signal and would lead to incorrect INP concentrations. The extremely smooth wafer surface allows for an unambiguous separation of particles from the background in the electron microscope. Each wafer is marked with three laser-engraved crosses near the edge, which span a 90° angle. These markers define a coordinate system, which allows for the precise localization of the ice-nucleation spots (Sect. 2.4).

After analysis, the wafer substrates are cleaned in a simple two-step process and can be reused subsequently. For this, wafers are pre-cleaned with ethanol and laboratory wipes (Kimtech Science, 7557, Kimberly-Clark) to eliminate oil residues from previous measurements and other coarse contamination. Then, in order to remove fine particles from the surface, the substrates are treated with a beam of dry ice crystals (Sno-Gun II, Va-Trans System, Inc.). The cleaning procedure is performed inside a particle free work space (SPECTEC, laminar flow box FBS). To verify the cleaning process, randomly selected cleaned wafers are analyz~~s~~ed in the ice nucleation chamber. However, even after thorough cleaning a small amount of ice formation can regularly be observed at temperatures at or below -30°C, constituting the background concentration and defining the limit of detection, which is in the order of 0.~~0~~1 L^{-1} of atmospheric air for a collection volume of 100 L.

2.2 Electrostatic Aerosol Collector

Aerosol is precipitated onto the substrates using an Electrostatic Aerosol Collector (EAC) (Klein et al. 2010). Several EACs have been deployed for the use in the laboratory (DeMott et al., 2018), in field campaigns (DeMott et al., 2024), for measurements with unmanned aerial vehicles (Schrod et al., 2017), and for long-term observations at research stations (Schrod et al., 2020b).~~,~~ The most recent ~~latter~~ version, which was also used in the case study (Sect. 3), ~~(~~PEAC7,~~)~~ is a programmable EAC (Schrod et al., 2016) designed for semi-automated operation for~~of~~ one week of daily sampling.~~Schrod et al. 2016). Several variants of the collector have been deployed for the use in the laboratory (DeMott et al. 2018), at field campaigns (Lacher et al., 2024, DeMott et al., 2024), for measurements with unmanned aerial vehicles (Schrod et al. 2017) and for long-term observations at research stations (Schrod et al., 2020b). The latter version (PEAC7) is a programmable EAC designed for semi-automated operation of one week of daily sampling.~~

Inside the collection unit, sample air passes through the corona discharge unit, which charges the particles negatively when a high voltage of about 12kV is applied. Charged aerosol particles follow the electric field to the grounded plate and are deposited on the silicon wafer substrate (Fig. 1~~-~~A). This sampling process leads to a rather homogeneous particle distribution on the wafer, which is of great importance both for the measurements in the ice nucleation chamber and for the later individual particle analysis by EM. ~~Nevertheless~~However, not all particles are deposited on the wafer during electrostatic precipitation, some are deposited elsewhere in the system. Characterization experiments determined a size-independent collection efficiency of 60 % in the 0.5-3 µm size range (Schrod et al., 2016). ~~Experimental details and a detailed description of the currently used PEAC7 can be found in Schrod et al. (2016).~~

2.3 FRIDGE

The FRankfurt Ice nucleation Deposition freezinG Experiment (FRIDGE) is an offline isostatic vacuum diffusion chamber in which the activation of atmospheric INPs and the associated growth of ice crystals can be observed and documented under laboratory conditions (Bundke et al., 2008; Klein et al. 2010~~, Schrod et al. 2016~~). The diffusion chamber addresses the deposition nucleation and condensation freezing modes (re-evaluated by Schrod et al., 2016), but the instrument can also be used in a different setup as a droplet freezing device to address the immersion freezing mode (~~e.g.,~~ Boose et al. 2016; Schrod et al., 2020a). As the immersion mode setup is not subject of our study, the following section describes the measurement procedure for the deposition nucleation and condensation freezing modes (schematic shown in Fig. 1B), with a particular emphasis on the desired coupling.

For coupling the INP ~~measurement~~activation experiment to the single particle analysis, it is important to keep the three laser-engraved crosses on the wafer surface visible during the FRIDGE measurement. The temperature sensor (PT1000) is therefore attached opposite to the middle cross, (see Fig.1 - ~~B1~~1B) ~~also with a little bit of oil.~~ A small amount of silicon oil is applied on the bottom of the wafer as well as on the temperature sensor ~~The sample substrate is placed on the cold stage inside the isothermal chamber, and a small amount of silicon oil is applied on the bottom of the wafer~~ to ensure good thermal contact and a homogeneous temperature distribution. ~~For coupling the INP measurement to the single particle analysis, it is important to keep the three laser engraved crosses on the wafer surface visible during the FRIDGE measurement. The temperature sensor (PT1000) is therefore attached opposite to the middle cross, (see Fig. 1B) also with a little bit of oil. After closing and evacuating the cold chamber, the system is adjusted to selected temperature and humidity conditions.~~ When the chamber is evacuated and the selected activation conditions are stable, ~~the valve to the water vapor source is opened and~~ the water vapor diffuses into the cold chamber, activating the INPs on the wafer surface. The growth of ice crystals is observed as a function of time (time step of 10 s) by a CCD camera (2/3" CCD ≥ 5 megapixels, 1 pixel ≈ 400 µm^2) placed above the reaction chamber. Ice crystals are identified by an image analysis software (LabView) comparing the brightness of new objects to a previously recorded reference image. Details can be found in Schrod et al. (2016). For the coupling ~~method~~ procedure it is beneficial to stop the growth of ice before individual ice crystals grow to large sizes or coalescence, because the determination of the ice crystal center (Sect. 2.4), which is assumed to be the position of the INP ~~(see Sect. 2.4.)~~, is more precise with small crystals. Additionally, this also reduces the spatial extent of potential particle drift during the ice crystal growth. By directly evaporating the ice crystals at the end of a measurement cycle with the objective of avoiding the liquid phase, the risk of possible particle drifts is also reduced.~~.~~

~~Once a measurement cycle is completed, further measurements can be performed on the same sample under different activation conditions.~~ As a routine, the wafers are measured in 12 cycles combining 3 temperatures (T = -20 °C, -25 °C, -30 °C) and four relative humidity (RH) settings each (RH = 95 %, 97 %, 99 %, 101 %). An efficient evacuation between measurement cycles is necessary to ensure the complete water evaporation from the particles to avoid pre-activation effects from residual water ~~/~~ ice in microscopic cavities on the particles surface (Jing et al., 2022). Based on the ice crystal numbers,

the collection volume and the ~~PEAK7~~ PEAC7 sampling efficiency, the INP concentration at different temperature and humidity settings is calculated.

For the subsequent ~~electron microscopy~~ EM with energy dispersive x-ray spectroscopy, it is important to completely remove the oil from the edge and underside of the wafer after the FRIDGE measurements, as otherwise the chemical analysis of the INPs can be influenced by the evaporating oil. Because of this oil-removing step, the edge and the area of the temperature sensor are excluded from further analysis.

2.4 Identification of ice crystal positions

In order to be able to match the ice crystals formed in FRIDGE to the corresponding ice-nucleating particles with SEM, the origin of each ice crystal must be located by a coordinate system based on the FRIDGE images. Therefore, ~~A~~a homogeneous distribution of ice crystals on the substrate with an adequate range of crystal density is favorable ~~for the coupling process. Furthermore, while working close to RH = 100 %, condensation may occur in the beginning of the FRIDGE measurements. The pictures showing condensation have to be removed, because otherwise the counting algorithm during the position identification is impeded.~~ The steps described below apply to such favored conditions.

The ice crystal positions are identified by image analysis using the internal particle analyzer of the free image processing software ImageJ (Schneider et al., 2012), with a minimum size of 30 pixels proven to be useful. The reference points of the coordinate system have to be defined manually b~~B~~y tagging the centers of the three crosses in a reference image ~~the reference points of the coordinate system are defined manually~~ as their non-uniformity ~~disturbs~~ prevents an automated approach. ~~The ice crystal positions are then tracked through the time series of images, and T~~the software identifies the image with the ~~maximum~~ highest number of ice crystals for each measurement cycle ~~is selected for further processing. and~~~~B~~~~based on differences in brightness, the software identifies~~ tags the ice crystal positions in the images as the center of the detected bright area. ~~After the ice crystal center identification,~~ These positions are translated into relative coordinates defined by the calibration marks. It can be assumed that this coordinate represents the position of the corresponding INP, since an approximately radially symmetric ice crystal growth can be observed in the range of the selected activation conditions in FRDGE. Nevertheless, a potentially imperfect radial symmetry of the ice crystal growth, coupled with the restricted resolution of the FRIDGE images (20 x 20 µm), may result in an uncertainty in the calculation of the ice crystal origin. As the size of an ice crystal increases, the probability and extent of such a non-symmetrical growth also increases. The quantification of this uncertainty proved to be difficult, as it depends on the symmetry deviation present. To reduce this uncertainty based on an imperfect radial symmetry, the ice crystal position calculation should be performed on the basis of FRIDGE images, that show the ice crystals in a state close to activation. ~~Additionally, a calibration image for the electron microscope is generated showing the previously marked center points of the three crosses.~~

Figure 2 shows a comparison between the number of ice crystals counted by FRIDGE and the number of ice crystal positions calculated for the SEM analysis. Usually, almost all ice crystal positions calculated by the counting algorithm can be ~~confirmed by the manual quality check~~related to real grown ice crystals, defined as clearly visible bright objects, which

continue to grow in the ice supersaturated regime as the measuring time progresses ~~(Fig. 2)~~. The few deviations are caused by various reasons. Higher numbers of ice crystal positions calculated for SEM can be caused by misclassifying areas with condensation, which may occur while working close to RH = 100 %. A lower number of ice crystal positions calculated for SEM is often caused by ice crystals that have grown together due to prolonged measurement in FRIDGE or by the presence of ice crystals in close proximity to one another, resulting in only one position for two or more crystals (see also Fig. S1). These Positions are excluded from further analysis. ~~.A reason for excluding a calculated coordinate from further analysis is a false identification as a result of ice crystals, which are very close to each other or have grown together. In rare cases, the coordinates of a specific ice crystal may differ slightly between separate measurement cycles due to variations in the extent and symmetry of the crystal growth.~~

~~To improve the quality of the data and keep the time-consuming SEM analysis as effective as possible the automatically calculated ice crystal positions are manually inspected to identify erroneous position markings. Therefore, an ice crystal is defined as the following: A clearly visible bright object, which continues to grow in the ice supersaturated regime as the measuring time progresses. Usually, almost all ice crystal positions calculated by the counting algorithm can be confirmed by the manual quality check (Fig. 2). A reason for excluding a calculated coordinate from further analysis is a false identification as a result of ice crystals, which are very close to each other or have grown together. In rare cases, the coordinates of a specific ice crystal may differ slightly between separate measurement cycles due to variations in the extent and symmetry of the crystal growth.~~

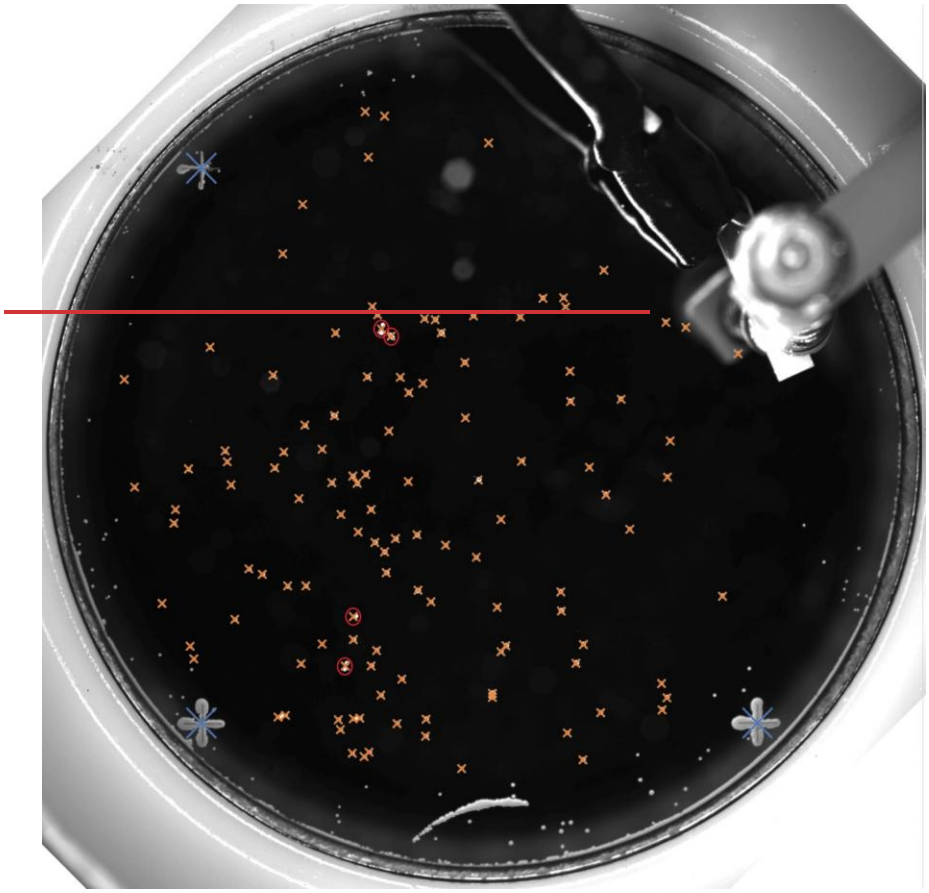

~~**Figure 2: Image of a silicon wafer from the FRIDGE diffusion chamber measurement with grown ice crystals (white dots) and the corresponding calculated positions for SEM (orange crosses). Miscalculated coordinates are marked with a red circle. The three laser-engraved crosses (at the large blue crosses) represent the reference points for the coordinate system. The edge of the sample substrate as well as the area around the temperature sensor are excluded from analysis.**~~

~~Figure 5 shows a comparison between the number of ice crystals counted by FRIDGE and the number of ice crystal positions calculated for the SEM analysis as described in chapter 2.4.~~

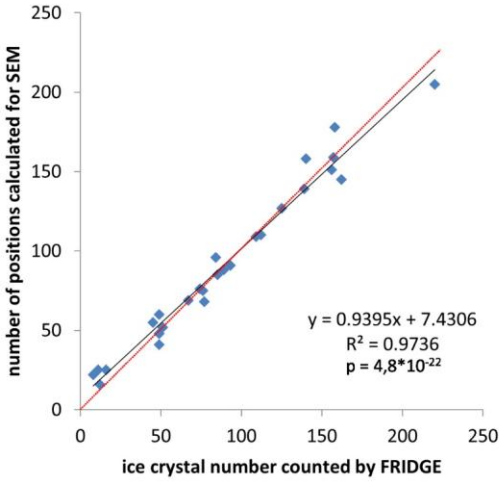

Figure 25: Comparison of ice crystal numbers detected by FRIDGE with the number of positions calculated for SEM analysis for the samples from CLACE/INUIT 2017 at the high-altitude research station Jungfraujoch (activated at T = -30°C and RH = 95 / 97 / 99 / 101 %). The 1:1-line is shown in red.

hat formatiert: Schriftart: 9 Pt.

In most cases, the numbers are almost identical, the few deviations are caused by various reasons. Higher numbers calculated for SEM are mainly caused by the counting of areas with condensation or by an incorrect wafer positioning in FRIDGE, resulting in counting ice crystal growth at the temperature sensor, which is normally excluded by the counting algorithm. A lower number of ice crystal positions calculated for SEM is often caused by ice crystals that have grown together due to prolonged measurement in FRIDGE, resulting in only one position for two crystals. Further improvements in the calculation of individual ice crystal positions can be achieved by specifically avoiding the sources of error previously mentioned.

2.5 Scanning Electron Microscopy

A Quanta 200 FEG Environmental Scanning Electron Microscope (ESEM) by FEI (Field Electron and Ion Company; Eindhoven, Netherlands) coupled to an energy dispersive X-ray detector (EDX) (EDAX, AMETEK, Tilburg, Netherlands) was used for analysis. The instrument is also equipped with an Everhardt-Thornley detector (ETD) which maps the topology of a particle by secondary electrons (SE) and a solid-state detector (SSD), providing the distribution of elements on the particle by backscattered electrons (BSE) giving information on homogeneous or heterogeneous distribution of elements and on inclusions. The EDX provides an elemental composition of an individual particle, which can be used to attribute the analyzed particles to different classes of composition and origin. As all analyses were carried out in high vacuum (10^{-6}

mbar), the instrument is referred to as ~~scanning electron microscope (~~SEM~~)~~ in the following. The acceleration voltage was 12.5 kV or 15 kV, the working distance was 10 mm as standard.

2.5.1 Coordinate calibration

As the internal SEM coordinate system is centered around the origin in the middle of the stage aligning the axes to the directions of mechanical movements ~~of the stage~~, it is necessary to perform a coordinate transformation to link the SEM coordinates ~~of the SEM~~ to the coordinates defined by the crosses in the previous step. Based on a calibration image, which indicates the marked center points from the previous ice crystal identification step (Sect. 2.4), these calibration points have to be transferred to the SEM.~~For that, the three crosses on the wafer are used as references in the SEM.~~ It is highly important to locate ~~their centers~~these points with high precision, since the position of each ice crystal in the subsequent analysis is based on this conversion. Manual calibration provides the highest precision, as the different physical imaging processes between the two instruments and the high magnification of the electron microscope in contrast to the limited resolution of the FRIDGE calibration picture, impair any precise automated calibration. Due to the limited resolution of the FRIDGE images of about 20 x 20 µm, the calibration has of course an uncertainty in the same order of magnitude.

2.5.2 ~~Individual particle analysis~~INP identification

Each ice crystal position, based on a real grown ice crystal, is inspected by SEM to identify the presence of particles. ~~that has been confirmed by the manual quality check is scanned for particles by SEM.~~ Given the uncertainties associated with the ice crystal identification process (Sect. 2.4) and the coordinate calibration (Sect. 2.5.1), it is crucial to consider not only the exact calculated coordinate but also the surrounding area. ~~Because the ice crystals are not grown perfectly symmetrical and the FRIDGE images have a limited resolution of about 20 x 20 µm per pixel, the calculated SEM coordinates have an uncertainty. Therefore, a radius of 50 µm around the calculated location is scanned.~~ This ~~radius~~ area must take into account the aforementioned ~~encompasses the stated~~ uncertainties ~~in order to find the INP while~~ and, at the same time, limit~~ing~~ the probability that several particles ~~to~~ will be observed ~~multiple particles~~ in the scanned area. In this context, a radius of 50 µm has proven to be useful. While the previously discussed uncertainties may suggest a lager radius to be beneficial, in fact, the high substrate loading often proves to be the limiting factor. Since the substrate loading depends strongly on the prevailing total aerosol concentration at the sampling location, the conditions for analysis can be optimized by adjusting the scanning radius for ~~specific circumstances~~different wafer loadings.

~~As a result, the method is limited in general with respect to the sampling volume of aerosol. The volume of air to be sampled must balance to effects: it must be sufficiently large to trap a statistically significant number of INPs on a wafer, but must avoid overloading in order to maintain enough distance between all - also the un-activated - particles (total wafer loading) to preserve unambiguity. Consequently, the fraction of INPs to the total aerosol impacts on the possible range of sampled~~

volumes. The method has worked reliably with a standard collection volume in the order of 100 L, despite a possibly high concentration of sub-100 nm particles being present in the sampled air. Presumably, there is a loss of volatile components during our sample collection and processing, enabling higher sampling volumes while limiting the method to the characterization of refractory particles. As the volatile particles are not known to be efficient INPs in the considered temperature range (Murray & Liu, 2022), we assume that this loss does not affect the results with respect to the analyzed particles. Since the substrate loading depends strongly on the prevailing total aerosol concentration at the sampling location, the conditions for analysis can be optimized by adjusting the scanning radius for specific circumstances.

While scanning the calculated locationice crystal position for particles, three cases can be distinguished: (1) one particle is found, (2) more than one particle is found, (3) no particle is found.

(1) If a one single particle is found within the specified radius, it is considered to be the thecorresponding INP identification is unambiguous and a single particle analysis is carried out. If the BSE-image, in which the contrast depends on chemistry, indicates chemical differences within the particle, multiple EDX spectra of the different areas are recorded (Fig. 3 and Fig. 4). Theis comprehensive single particle analysis (Sect. 2.6) enables the identification of mixing state and distinct morphological patterns on the particle surface that may physico-chemical properties that may be pertinent to ice formation.

(2) If more than one particle is found identified within the defined area around the coordinate, it is not possible to make a definite allocation of the INP. Tthese positions have to be excluded from the are usually excluded from analysis. In case all particles in the scanning area have the same chemical composition, the information about the particle class relevant to ice formation is still obtained. However, no clear statement on the size and specific features of one unique INP can be made.

(3) If no particle is foundIn the absence of a particle within the 50 µm radius, these blank positions are usually neglected as welltypically disregarded. A blank position may be the consequence of possible particle drift during the processing in FRIDGE (Sect. 2.3), or the result of an erroneous calculation of the ice crystal origin (Sect. 2.4). HoweverNevertheless, if in instances where thethe substrate loading is low is low, extending the screening radius (e.g., to 100 µm) in the case of a blank position can may be beneficial help toin increasinge the number of identified INPs. It is important to consider this extension for the entire sample, otherwise the unique identification criteria of an INP are no longer consistent.

Figure 3 illustrates a result from the INP identification step with the SEM, based on the corresponding FRIDGE picture with the grown ice crystals.

The number of INPs that can be unambiguously attributed to an ice crystal origin is significantly influenced by the total wafer loading, which is determined by the sampling parameters (e.g., flow rate, sampling time, deposition efficiency) in combination with the aerosol concentration present. However, even if the aerosol concentration is known, it is difficult to specify a suitable collection volume in advance, as the ratio of potential INPs to the total aerosol also plays a role. This ratio is variable and usually unknown prior to measurement. As a result, the amount of atmospheric aerosol and the proportion of INPs deposited on a wafer are highly variable. This variability is also seen in the identification rates, which is why it would be misleading to give an average identification rate for the method presented. However, a specific identification rate for the

hat formatiert: Englisch (Vereinigte Staaten)

hat formatiert: Englisch (Vereinigte Staaten)

hat formatiert: Englisch (Vereinigte Staaten)

case study conducted at the high-altitude research station Jungfraujoch (Sect. 3) can be given here as a guideline. The average INP identification rate was calculated to be 30% (ranging from 13 % to 50 %). Furthermore, the study identified the presence of multiple particles at 45 % of the locations (ranging from 7 % to 81 %), while the remaining 25 % (ranging from 2 % to 66 %) were found to be blank positions.

Based on the uncertainties and assumptions discussed, many positions and potential INPs are excluded from further analysis, which leads to the limited number of identified INPs per sample. However, these INPs are identified with a high degree of accuracy as we know that ice formation has taken place on the substrate at their position. In most cases, the small number of clearly identified INPs still allows general statements to be made, e.g., about the most frequently occurring characteristics of INPs (e.g., predominantly silicates or predominantly sub-µm particles), but often no general statement about rarely occurring subgroups of INPs are possible (see Sect.3).

~~Depending on the total wafer loading, the number of INPs identified by SEM is usually smaller than the number of ice crystals grown during the FRDIGE measurement.~~

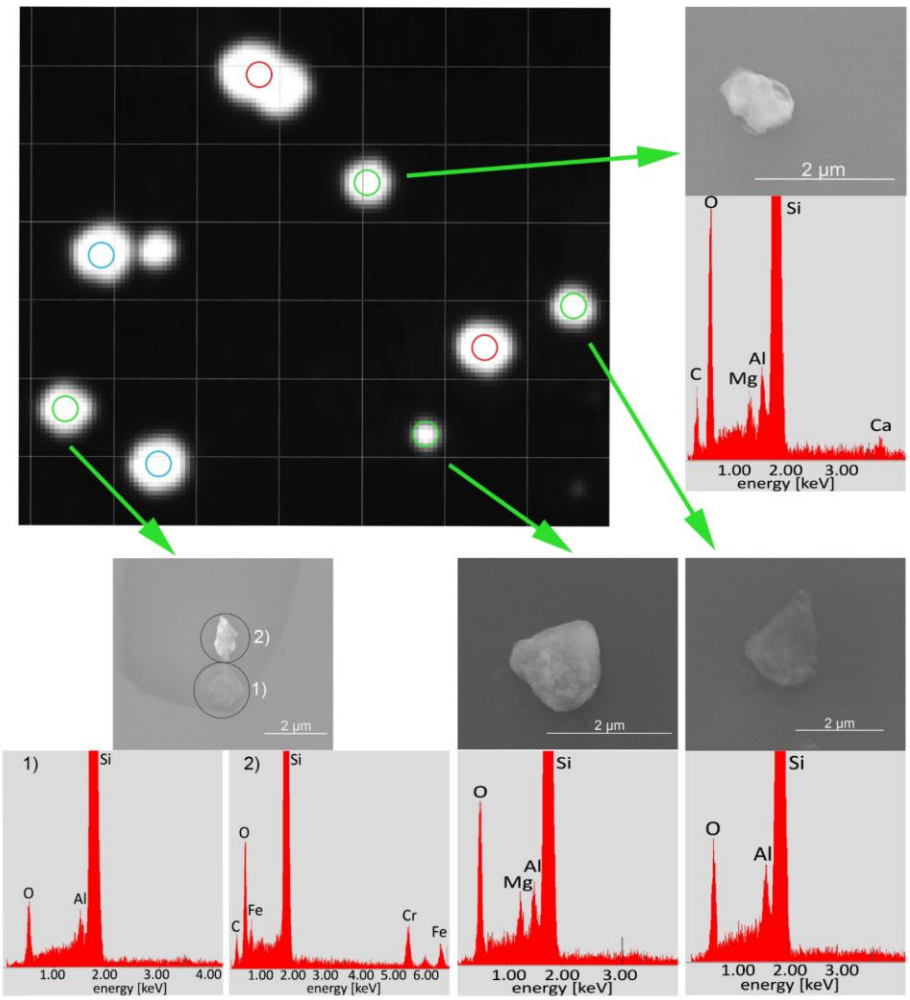

460

Figure 3: FRIDGE picture (resolution 20 x 20 µm) showing grown ice crystals including one coalesced crystal (top center). The corresponding scan radius of 50 µm from SEM is shown by the colored circles: Blank positions (red), multiple particle positions (blue) and identified INPs (green). However, one ice crystal was not detected by the ice crystal identification software. For the

Formatiert: Zeilenabstand: einfach

identified INPs, the corresponding pictures and EDX spectra are shown. For one particle (bottom left), the BSE image indicates a different chemical composition, so two spectra were recorded.

~~The size of each identified INP is determined by calculating the projected area diameter (d_{pa}) from the SE- / BSE images. Therefore, the particle is regarded as an ellipse and the dimensions of its major and minor axis are determined in order to subsequently calculate the diameter of an equivalent circle, which is referred to as d_{pa}. The calculated diameters represent the particle size obtained as a result in the last stage of the analysis and may therefore differ from the size of the initially activated INPs. Volatile components within a sample (e.g., water) may evaporate during the analysis procedure possibly changing the appearance of the sampled particles. Figure 1 C shows a schematic of this SEM step with a BSE image / EDX spectra and the chemically resolved size distribution as a final result.~~

2.6 ~~Chemical classification~~Individual particle analysis

The analysis by SEM and EDX is an ~~excellent~~ efficient ~~way~~ method ~~of~~ for characterizing INPs in detail, as it provides information on elemental composition and distribution as well as on morphology and surface properties.. With this detailed information, it is possible, for example, to determine the mixing state of a particle (see Fig. 3 and Fig. 4). ~~as i~~In ~~addition to the chemical analysis, which provides information about the elemental composition of an INP, t~~he morphological ~~characterization~~ information can be used for source apportionment (e.g., for biological particles, soot, spherical particles from high temperature processes). ~~to identify surface properties relevant to ice nucleation.~~

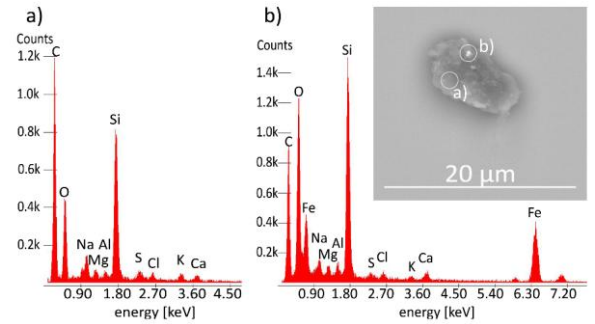

Figure 4: EDX spectra and BSE image of a C-rich INP (a) with Fe-rich areas (b).

The size of the INPs is determined in the last step of the coupling method from the SE/BSE pictures. The INPs have been processed in FRIDGE (multiple activation/evacuation cycles) and they were analyzed in a high vacuum under the electron beam. Therefore, the morphology of the particles may have undergone alterations. This may be especially the case for

hat formatiert: Deutsch (Deutschland)

Formatiert: Zentriert

hat formatiert: Schriftfarbe: Automatisch

hat formatiert: Schriftfarbe: Automatisch

hat formatiert: Schriftfarbe: Automatisch

soluble/volatile components within a sample, which may evaporate during the analysis procedure. It can be assumed that these changes are of minor importance for most of the INPs classes that can be determined using this method.

~~In our specific case, the silicon content cannot be quantified as we are working on a Si substrate and we therefore always obtain a Si background signal in the spectrum. In the case of very small particles the signal intensity with respect to this background signal may be too weak or missing, so there is no possibility to characterize them chemically. The same applies for particles with an original droplet shape as well as for residues that spread more like a film. Instability with respect to the electron beam also leads to limited detection of particle properties.~~

In the following section we define ~~the particle classes~~ a classification scheme~~which were used to categorize the identified INPs sampled at the high-altitude research station Jungfraujoch in winter 2017 (see Sect. 3).~~, which is mainly based on elemental composition (Fig. 5) and in some cases on the morphology of particles (Fig. 7). ~~In the following we present a brief description of each group, focusing only on the major elements and properties. As the particle composition depends on the sampling location, the INP classification scheme (supplementary material – Fig. S1) for other locations may be different.~~The subgroups defined in Fig. 5 can be summarized in three main groups (mineral particles, carbonaceous particles and other particles).

It should be noted, however, that it is not possible to quantify the silicon content of a particle with this method. Given that we are working on a silicon substrate, a Si background signal in the resulting spectrum is always present. This may limit the chemical characterization of particles with a very small size, as their element signals with respect to the background signal may be insufficient. Instability with respect to the electron beam also leads to limited detection of particle properties.

Based on the research question or the occurrence of specific particle classes at the sampling site, the classification scheme may be adapted.

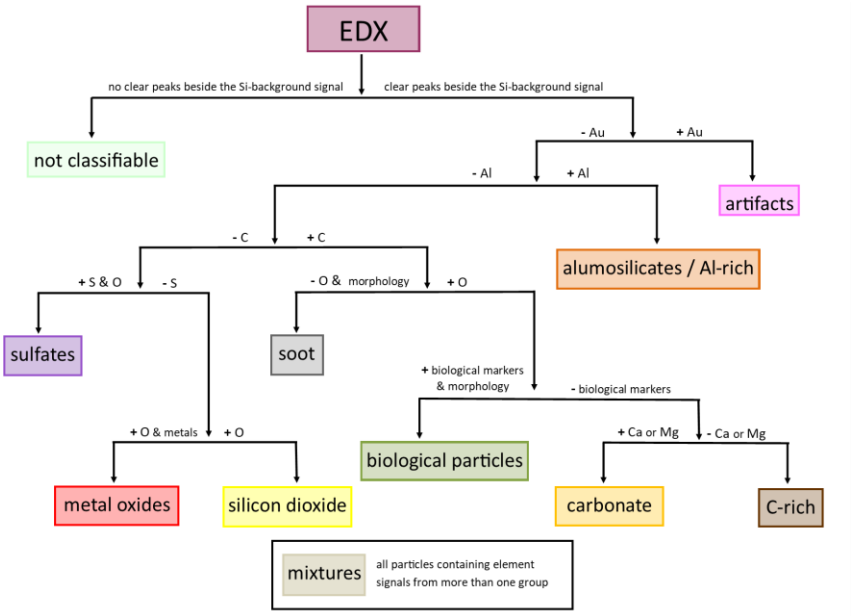

Figure 5: INP classification scheme.

Mineral components

Aluminosilicates / Al-rich particles, carbonates and silicon dioxide are summarized as mineral components. Typically, their irregular structure indicates a geogenic origin.

The *aluminosilicate / Al-rich* group is identified based on the Al signal and represents a combined group, as it is not possible to quantify the silicon content of a particle~~includes all particles which have aluminum (and oxygen) as their main detectable elements – due to the Si wafer substrate, there is always a large peak from Si present which cannot be~~. The dominating source for aluminosilicates in the atmosphere is mineral dust from arid and semi-arid regions, while Al-dominated particles are usually rare (Okada & Kai, 2004; Kandler et al., 2007). ~~quantified. Nearly all~~ In case of aluminosilicates, the particles may contain several minor elements (e.g., Na, Mg, K, Ca, Fe) in different ratios (Fig. 6) ~~(e.g., Na, Mg, K, Ca, Fe)~~, depending on the minerals from which they originate. ~~Most particles are irregular and t~~Their internal element distribution ~~is~~ may be not homogeneous. This method can therefore be used to estimate the abundance of individual mineral components in the INP fraction, potentially identifying an enrichment of highly effective ice nucleating particles (e.g., K-feldspar).~~The dominating~~

Formatiert: Zentriert

hat formatiert: Schriftfarbe: Automatisch

hat formatiert: Schriftfarbe: Automatisch

source for aluminosilicates in the atmosphere is mineral dust from arid and semi-arid regions, while Al-dominated particles are usually rare (e.g. Okada & Kai, 2004; Kandler et al., 2007).

The spectra of the *Cc*arbonates group include, can contain, in addition to carbon and oxygen, different counterions (e.g., calcium and/or magnesium), based on the mineralogical origin as counterions. The irregular shaped particles can be related to geogenic origin (e.g., calcite, dolomite).

If only oxygen can be detected alongside silicon, it can be assumed that it is *Ss*ilicon dioxide (quartz)is identified by the presence of only oxygen alongside - the not quantifiable - silicon, however it is not possible to make a reliable statement about the silicon content of the particles. A distinction between different particle sources can be made on the basis of their morphology. While Most most geogenic quartz particles show irregular shapes with typical sharp edges (Whalley and Krinsley, 1974). aAnthropogenic SiO_2 particles from industrial high temperature processes show more spherical shapes. Fragments of the wafers are can be clearly identified as artifacts by their sharp edges, glassy fracture and lack of oxygen signal.

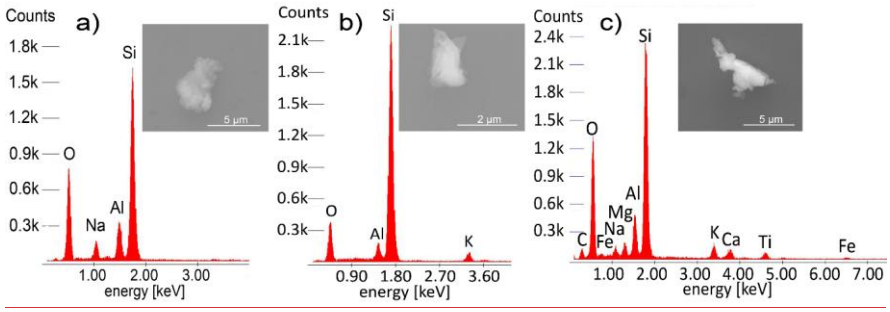

Figure 6: EDX spectra and SE-images of various aluminosilicates: a) Na-containing aluminosilicate; b) K-containing aluminosilicate; c) complex aluminosilicate

Carbonaceous containing particles

All particles with carbon as their main element are combined as carbonaceous particles.

In addition to a high carbon content, tThe group of *biological particles*, which includes plant debris, pollen, bacteria and fungal spores as well as their fragments, is can be characterized by the presence of biogenic trace elements such as phosphorusP, potassiumK, magnesiumMg, calciumCa, sodiumNa, etc. (Ebert et al. 2000) and by their characteristic appearancemorphology. Based on our criteria, particles are only classified as biological if the bulk particle fulfills these criteria. The group of biological particles includes plant debris, pollen, bacteria and fungal spores as well as their fragments.

hat formatiert: Schriftfarbe: Automatisch

Formatiert: Zentriert

In many cases, *soot* particles can be clearly assigned based on their typical morphology (Fig. 7), which often shows long chains or larger agglomerates of small, spherical primary particles (Sorensen & Feke 1996). If it is not possible to characterize them by their morphology, they can be identified ~~Due to particle aging in the atmosphere or small particle sizes some of the soot particles cannot be classified by their morphology. In these cases, they have to be characterized~~ by their very low oxygen content compared to carbon. ~~All particles with a high carbon content, which cannot be classified as soot by the previous criteria are classified as C-rich. The proportion of soot therefore only represents a lower limit.~~

The *C-rich group* contains all particles with high carbon ~~peaks in their spectra~~, which cannot be clearly classified as biological particles or soot. ~~Since some particles from those two groups can be assigned as C-rich, this class~~It may ~~contain~~ also contain components from all other ~~refractory~~ organic ~~parts~~ particles in the atmosphere, which can be analyzed with this method. ~~Therefore, the morphological variability of these particles is high.~~

Other particle classes

All subgroups that cannot be clearly assigned to one of the two previous main groups are summarized as other particle classes.

The *metal oxides* are characterized by the presence of oxygen and a corresponding metal (except Al, which ich assigned to the previous aluminosilicate / Al-rich particles group)~~not classified into a previous group, which is in our case primarily iron~~. Metal oxides can originate from geogenic minerals as well as from anthropogenic sources, that is why we refrain from clearly assigning this group to mineral particles. The morphology of these particles can be either irregular (e.g., natural mineral du~~r~~st, anthropogenic urban dust), or spherical, with the latter possibly originating from high-temperature processes (e.g., coal combustion) or aircraft emissions. ~~Since no final source identification of the metal oxides could be performed, we refrain from clearly assigning this group to a mineral origin.~~

~~The particles of the~~ *~~S~~sulfate*s ~~*group*~~ are mainly characterized by the presence of sulfur and oxygen. This method can detect only beam-stable sulfates reliably. Ammonium sulfate, for example, is not beam-stable during the analysis and therefore cannot be detected reliably. ~~Calcium and, in some cases, potassium are the primary counterions.~~ The ~~appearance~~ morphology of these particles varies from clean crystallization to agglomerates and irregular shapes, depending on their source and formation processes. Besides the geogenic sources (minerals like gypsum or anhydride), possible anthropogenic sources are industrial processes (mainly coal combustion), flue gas desulfurization and fertilizers. ~~This method can detect only beam-stable sulfates reliably. Ammonium sulfate, for example, is not beam-stable during the analysis and therefore cannot be detected reliably.~~ Due to the diversity of their possible sources and characteristics, we abstain from classifying them as minerals, although some of them may have a mineral origin.

All particles which are containing elements from more than one of the groups presented are assigned to *mixtures*. ~~The group of *mixtures* includes particles which are containing elements from more than one of the groups presented. The most abundant~~

hat formatiert: Schriftart: 10 Pt.

hat formatiert: Schriftart: Kursiv

~~mixtures feature in addition to an Al peak, which is characteristic for the aluminosilicate / Al-rich group, also a distinct carbon peak (C/Al ratio > 0.2). This can be an indication of soil dust, which contains carbonaceous material in addition to aluminosilicate / Al-rich minerals. Apart from this, the described composition can also be generated by mixing or coating with carbonaceous materials during particle aging in the atmosphere. The morphology of the particles is as variable as the composition and is mostly irregular.~~

Particles with gold deposits are classified as *artifacts* due to the use of gold wires as electrodes during the sampling process.

~~In rare cases, traces of gold were found on single particles. Since gold wires are used as electrodes to initiate the discharge during the sampling process, these particles were categorized as sampling *artifacts* and therefore excluded from further analysis.~~

~~All particles which can be clearly identified as INPs based on their position, but do not provide clear element peaks beside the silicon background signal are grouped as *not classifiable*.~~

At this point, it should also be noted that our findings revealed an absence of small volatile compounds on the wafers in the EM, which are typically present in larger numbers in the total aerosol. Presumably, there is a loss of these components during sampling collection or processing. However, as these volatile particles are not known to be efficient INPs in the considered temperature range (Murray & Liu, 2022), it can be assumed that their absence does not significantly affect the results.

~~An overview of all particle groups with example pictures and EDX spectra is given in Fig. 3.~~

hat formatiert: Schriftfarbe: Automatisch
hat formatiert: Schriftfarbe: Automatisch
hat formatiert: Schriftfarbe: Automatisch
hat formatiert: Schriftfarbe: Automatisch
hat formatiert: Schriftfarbe: Automatisch
hat formatiert: Schriftfarbe: Automatisch
hat formatiert: Schriftfarbe: Automatisch
hat formatiert: Schriftfarbe: Text 2

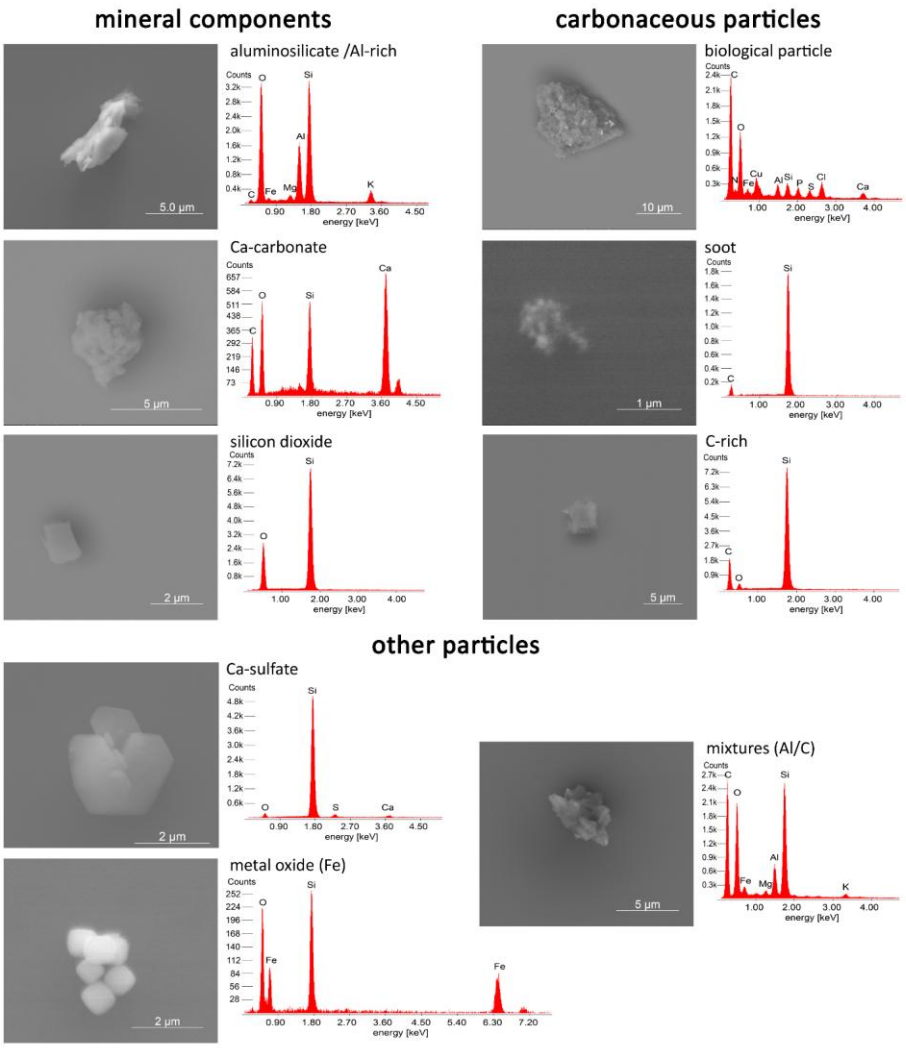
mineral components
carbonaceous particles
aluminosilicate /Al-rich
biological particle
Ca-carbonate
soot
silicon dioxide
C-rich
other particles
Ca-sulfate
mixtures (Al/C)
metal oxide (Fe)
5.0 µm
10 µm
5 µm
1 µm
2 µm
5 µm
2 µm
5 µm
2 µm
energy [keV]

600

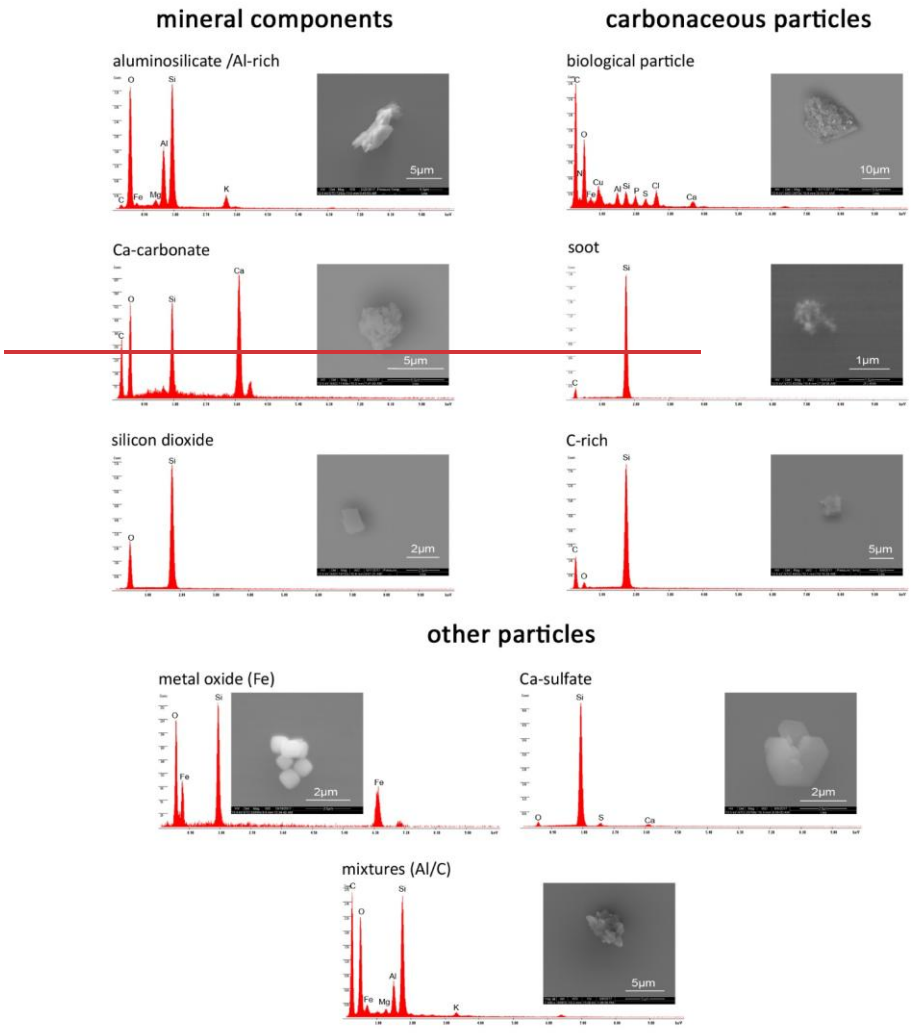

Figure 73: Overview of representative EDX spectra and corresponding ~~SE- / BSE-~~images for each particle class ~~from CLACE / INUIT 2017 at the high-altitude research station Jungfraujoch~~.

3 Case Study: Results from the CLACE ~~/~~ INUIT campaign at the high-altitude research station Jungfraujoch in 2017

3.1 Sampling site

The high-altitude research station ~~Jungfraujoch (~~JFJ~~)~~ is located in the Swiss Alps at 3580 m above sea level between the mountain peaks of Mönch and Jungfrau. A general description of the station can be found in Bukowiecki et al. (2016). The samples were collected during the Cloud and Aerosol Characterization Experiment / Ice Nucleation Research Unit campaign (CLACE ~~/~~ INUIT 2017) between January 21 and February 25 2017. During winter, the station is 60 % of the time in the free troposphere (FT) (Herrmann et al., 2015), which enables characterization of the global background aerosol. A temporary influence of the planetary boundary layer is possible at any time of the year. According to Baltensperger et al. (1998) the station is in clouds (mixed-phase and ice) 40 % of the time. Since the average temperature did not fall below -15 °C during the sampling period, we assume that most INPs with activation temperatures of -20 °C to -30 °C were not activated under the prevailing environmental conditions. Even though some of them might have been activated previously in higher clouds, sampling under cloudy conditions likely does not introduce a large bias due to previously activated INPs. Aerosol sampling for the FRIDGE experiment was conducted downstream of the GAW total inlet (Lacher et al., 2021).

3.2 INP concentration & sample selection

Figure 8 illustrates the evolution of INP concentrations across the three activation temperatures, as determined by FRIDGE. The concentration for each sample is calculated on the basis of one measurement. The relative error of the counting uncertainty for individual measurements is 20 % (Schrod et al., 2016), so the error of the concentrations given here is also in this range. The concentrations observed at each temperature exhibited fluctuations of approximately one order of magnitude across the entire campaign period. Towards the end of the campaign, a Saharan dust event (SDE) was identified, which resulted in an increase in INP concentration at both -25 °C and -30 °C. This was not the case for -20 °C, as Saharan dust particles primarily activate as INPs at temperatures below -20 °C (Niemand et al., 2012, Murray et al., 2012). Since the INP concentration for -20 °C and -25 °C was sometimes very low during the campaign ~~(Fig. 4)~~, we focus on the INPs activated at -30 °C ~~($c_{INP,-30}$)~~ for the single particle analysis. Their concentration varied between 0.1 and 1 stdL^{-1} for most of the time. Based on the experience that most ice nuclei active at warmer temperatures also activate at colder temperatures, it can be assumed that only a few INPs are neglected due to limiting the analysis to INPs activated at -30 °C.

hat formatiert: Schriftart: Nicht Fett

hat formatiert: Schriftart: Nicht Fett

hat formatiert: Schriftfarbe: Automatisch

hat formatiert: Schriftfarbe: Automatisch

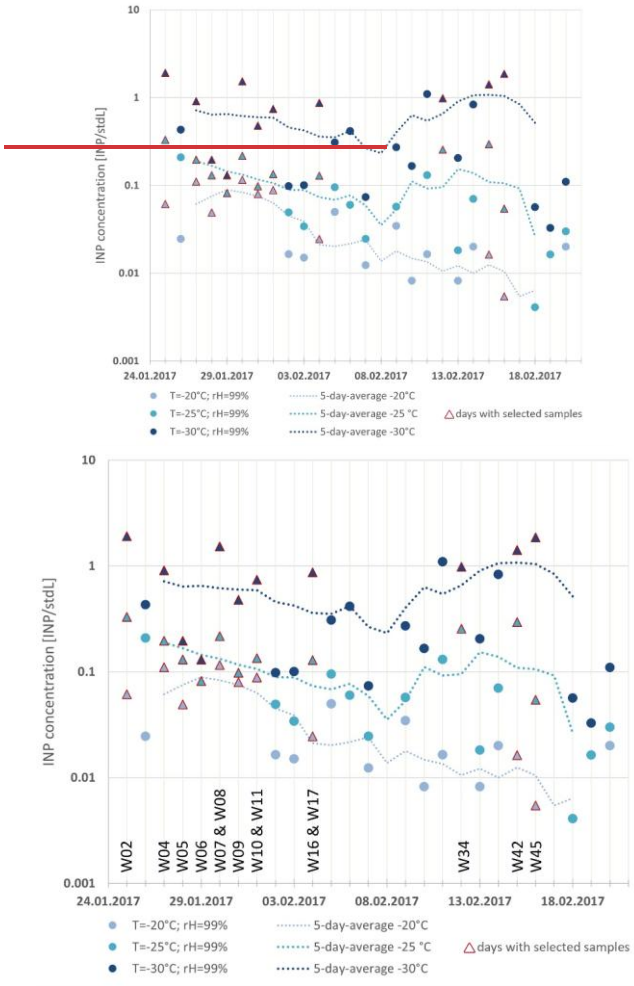

Figure 84: INP concentrations (deposition nucleation / condensation mode freezing) calculated from the FRIDGE measurements at RH = 99 % (for days with more than one sample, an average value was calculated). Days with analyzed samples are indicated by triangles and the corresponding sample numbers. The 5-day running -average concentration is shown by the dotted lines (the figure ~~was modified according to~~is adapted from Weber (2019)).

The $c_{INP,-30}$ varied between 0.1 and 1 $stdL^{-1}$ for most of the campaign. A Saharan dust event (SDE) was encountered during the end of the campaign. The INP concentrations for -25°C and -30°C followed the same trend in general, including a marked increase in the INP concentration during the SDE. This was not the case for -20 °C, because Saharan dust particles primarily activate as INPs at temperatures below -20°C. A total of 14 substrates out of a were selected from the larger set of samples obtained from the measurement campaign for analysis using were analyzed with the coupling method here presented method herein. The particular samples were chosen because of based on their ice crystal abundance and homogeneous distribution on the substrate during the FRIDGE measurements. These samples are indicated by the corresponding sample number and triangles in Fig. 84. Based on the experience that most ice nuclei active at warmer temperatures also activate at colder temperatures, it can be assumed that only a few INPs are neglected due to limiting the analysis to INPs activated at -30°C.

3.3 Method evaluation

Between 8 and 220 ice crystals had grown on the substrate surface of each wafer during the ice nucleation experiments in FRIDGE at -30°C. Figure 5 shows a comparison between the number of ice crystals counted by FRIDGE and the number of ice crystal positions calculated for the SEM analysis as described in chapter 2.4.

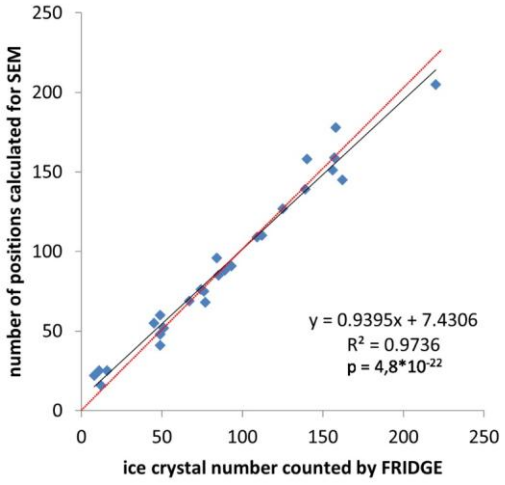

Figure 5: Comparison of ice crystal numbers detected by FRIDGE with the number of positions calculated for SEM analysis for the samples from CLACE/INUIT 2017 at the high-altitude research station Jungfraujoch (activated at T = -30°C and RH = 95 / 97 / 99 / 101 %).

Formatiert: Block

Formatiert: Zeilenabstand: 1,5 Zeilen

~~In most cases, the numbers are almost identical, the few deviations are caused by various reasons. Higher numbers calculated for SEM are mainly caused by the counting of areas with condensation or by an incorrect wafer positioning in FRIDGE, resulting in counting ice crystal growth at the temperature sensor, which is normally excluded by the counting algorithm. A lower number of ice crystal positions calculated for SEM is often caused by ice crystals that have grown together due to prolonged measurement in FRIDGE, resulting in only one position for two crystals. Further improvements in the calculation of individual ice crystal positions can be achieved by specifically avoiding the sources of error previously mentioned.~~

~~In the end~~Overall, based on the parameters described in Sect. 2.5.2~~.~~, we were able to clearly identify and characterize the associated INPs for 200 ice crystals. Although the number of identified INPs appears comparatively low for a campaign period of five weeks, these INPs were identified with a high degree of reliability (Sect. 2.5.2). The small number of particles identified bears the risk that individual, time-limited variations occurring randomly during the sampling periods may influence the resulting total composition to a certain degree. It should therefore be noted that the results presented below may not comprehensively reflect the main composition of the INPs over the entire campaign period. Nevertheless, it can be shown that the method provides valid results for the main groups of INPs (see confidence intervals for Fig. 9 in the supplement (Tab. S2)). ~~, which is a fraction of 15% of the total number of ice crystals grown on the 14 wafers. Unfortunately, at the time of the study, only a restricted area of 4 cm² in the middle of the wafer was analyzed by SEM, which corresponds to about half of the total analyzable area. Due to the oil removal process that has to be done before SEM, the edge of the wafer and the aera of the temperature sensor have to be excluded. Taking the whole analyzable area into account, the unambiguous INP identification rate can be calculated at 30% for this campaign. We found more than one particle at 40% of the locations, at the remaining 30% we found blank positions. As these numbers depend strongly on the total wafer loading, which correlates to the total particle concentration and the activated fraction in the sampled volume as explained in Sect. 2.5.2., the identification rates given above apply only for the specific conditions encountered during the CLACE / INUIT 2017 campaign. In more recent studies, the area of analysis has been extended to the total analyzable wafer surface, to increase the total number of identified INPs, yielding better statistics.~~

3.~~3~~4 INP chemistry

The 200 particles identified as INP in the vicinity of the calculated coordinate were grouped into particle classes according to the classification scheme shown in Sect. 2.6. One particle with attached gold traces was classified as an artifact and therefore excluded from further discussions. ~~Figure 6 shows the~~ The ~~total~~ chemical composition of the remaining 199 INPs activated at -30 °C is shown in Fig. 9.~~over the entire campaign period.~~ Due to the limited number of identified INPs per sample (Fig. S3), mapping daily fluctuations is not possible for this campaign. Figure 9a) provides the chemical composition for all INPs sampled over the entire campaign period, within the restrictions mentioned in Sect. 3.2. Figure 9b) illustrates the methods efficacy in representing larger INP-relevant trends. Despite the small number of INPs, the SDE can be clearly recognized by

a different chemical composition of the INPs from this period (confidence intervals are given in the supplement (Tab. S2)). ~~per sample, a detailed meteorological interpretation of results is not feasible. Included are samples from both cloudy and clear sky, as well as air masses from different regions and a SDE. The INP chemical composition of the individual samples can be found in the Supplementary Material (Fig. S2).~~

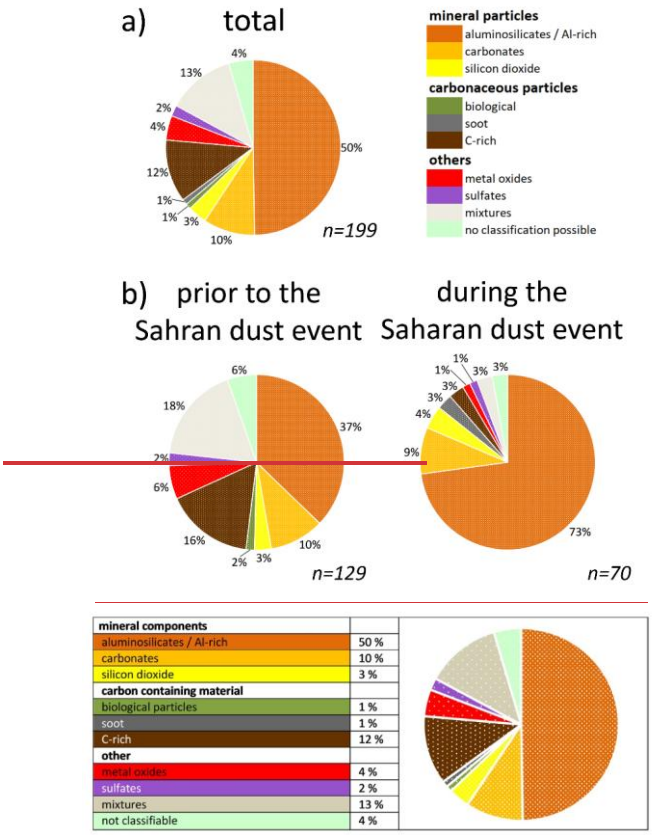

Figure ~~9~~6: ~~Total c~~Chemical INP composition ~~(artifact excluded; n = 199)~~ with the number of analyzed particles (n) from CLACE/INUIT 2017 at the high-altitude research station Jungfraujoch (activated at T = -30 °C and RH = ~~95 / 97 /~~ 99 / ~~/~~ 101 %; RH = 95 / 97 % was chosen for one sample due to cluster formation at higher RH). a) total

composition over the whole campaign period; b) composition prior to and during a Saharan dust event. For confidence intervals see supplement Tab. S2.

Mineral components

The analyzed INPs sampled at the high-altitude research station JFJ in January and February 2017 were found to be predominantly composed of ~~dominated by~~ mineral components (63 % in total ~~63 %~~). Their proportion is 50 % prior to the SDE, rising to 86 % during the SDE. Among these, the aluminosilicate / Al-rich group ~~was~~ increases from 37 % to 73 %, whereas the carbonates and the silicon dioxide have almost the same proportion. Throughout the entire campaign period, aluminosilicates / Al-rich particles were most prevalent, compromising ~~with~~ 50 % of the total identified particles. ~~and was~~ These particles were present~~detected~~ in all individual samples, ~~(~~except for W10, which had only one identified INP in total~~)~~. ~~Very high abundances of these geogenic aluminosilicate / Al-rich particles were found especially for three samples taken during the SDE (W34 / W42 / W45) but also for two samples before the SDE (W2 & W17). Beside Al and Si, mostly Fe, K, Mg, C and Na showed up as minor elements.~~ Carbonates ~~particles~~ were detected in 9 individual samples (total contribution of 10 %) with Ca as the main counter ion. ~~Two carbonates showed indications of former droplet shape, suggesting that they originally existed as airborne droplets.~~ *Silicon dioxide* particles contributed 3 % of all identified INPs, with~~. Particles with~~ mostly irregular shapes indicating a geogenic origin ~~were found~~ in three samples~~., all spherical particles derived from one sample (W45). Since spherical particles mostly originate from high temperature processes, maybe this sample was influenced by an anthropogenic SiO_2 source (regional or long-range transport).~~

These findings are in good agreement with results reported from other INP/IR measurements at the same site. Eriksen Hammer et al. (2018) and Lacher et al. (2021) observed the presence of mineral particles in comparable quantities during the same research campaign, despite analyzing IR activated between -10 °C and -18 °C. In previous campaigns Worringen et al. (2015) also identified terrigenous material as a significant contributor to ice nucleation at JFJ and Kamphus et al. (2010) observed a significant enrichment in minerals in IR compared to the total aerosol.

*Carbon*aceous ~~containing~~ *particles*

The carbon-dominated particles represented 14 % of the total INP composition during the CLACE ~~//~~ INUIT 2017 campaign. Only ~~a very small percentage~~some single particles (1 % in each case) could be clearly assigned to a biological origin or soot. The remaining 12 % were classified as C-rich, and both biological ~~fractions~~ material and soot, as well as any other carbonaceous particles existing in the atmosphere, may be included in this group. The fraction of carbonaceous particles decreased from 18 % before the SDE to only 6 % during the SDE.

hat formatiert: Schriftfarbe: Rot

hat formatiert: Schriftart: Nicht Kursiv

hat formatiert: Schriftart: Nicht Kursiv

Carbonaceous material was also identified as minor component in INPs/IRs at the high-altitude research station JFJ during winter 2013 by Worringen et al. (2015) as well as by Eriksen Hammer et al. (2018) and Lacher et al. (2021) for January and February 2017.

Other particle classes

During the CLACE / INUIT 2017 campaign ~~at the high-altitude research station JFJ~~ metal oxides, which were primarily iron oxide, were found ~~in 5 samples (~~with a proportion of 4 % in total~~)~~. ~~These were primarily iron oxide, but some single oxides with other metal ions (magnesium and zinc) have also been detected.~~ A few particles within this group contained iron together with Ni and Cr as alloying elements that could be characteristic for steel. An anthropogenic origin or a local source from the station for these particles is assumed, but not confirmed. Apart from some single metal oxides with spherical shapes, most of them showed irregular shapes which may hint at a geogenic origin. Metallic particles and metal oxides have also been identified as a minor ice-forming compound by other studies conducted at the high-altitude research station JFJ (Kamphus et al., 2010; Worringen et al., 2015; Eriksen Hammer et al., 2018; Lacher et al., 2021). Ebert et al. (2011) also found metal oxides in their IRs and classified them primarily as iron oxide, which is consistent with our results.

Sulfates were rare (2 %) ~~and only present in three samples~~ with Ca as the main counterion.~~:~~ Their morphology indicates a predominantly mineral origin. ~~The potassium sulfate appeared to be droplet-shaped, indicating that it was originally present as a droplet in the air.~~

The most abundant particle type of our mixture group features in addition to an Al peak, which is characteristic for the aluminosilicate / Al-rich group, also a distinct carbon peak (C/Al-ratio > 0.2). ~~The mixed particles group contained 13 % of all identified INPs. Besides two metal oxides with additional carbon signals and two particles with signals from Fe and S, the other mixed particles showed element signals from aluminosilicate / Al-rich particles (Al as a tracer in combination with characteristic minor elements) but also a distinct signal for carbon.~~ Most of these particles ~~this Al/C-mix INPs~~ had a stronger Al-Peak with respect to the carbon peak (C/Al-ratio < 1). This Al/C-mixture may be an indication of soil dust, which contains carbonaceous material in addition to aluminosilicate / Al-rich minerals. In contrast to the aluminosilicate / Al-rich group these Al/C-mixed particles were found primarily in samples without influence of the SDE (18 % vs. 3 % during SDE), potentially pointing to a different origin of the air masses and thus a different type of mineral material (e.g., soil dust) which was transported to the station. Apart from this, the described composition can also be generated by mixing or coating with carbonaceous materials during particle aging in the atmosphere~~Another possible reason could be that the particles have been processed during their atmospheric exposure and~~, in contrast to the freshly emitted Saharan d~~D~~ust~~, are mixed with other carbonaceous components~~. Such a mixed group at the high-altitude research station JFJ was also characterized by previous studies (Worringen et al., 2015; Ebert et al., 2011). Lacher et al. (2021) reported also that many of their mineral dust particles from the CLACE/INUIT 2017 campaign showed signals of biological material, which may be equivalent to the mixed INPs in our study.

hat formatiert: Schriftart: Nicht Kursiv

hat formatiert: Schriftart: Nicht Kursiv

For 4 % of all particles which can be clearly identified as INPs based on their position, ~~clearly localized particles~~ no chemical classification could be performed as outlined in Sect. 2.~~6~~5.2.

It is generally difficult to make direct comparisons between the results of different INP/IR measurement techniques, as the results can vary significantly depending on the sampling configuration, ice nucleation activation conditions, and the classification schemes used for each instrumentation. Despite these constraints and with only a limited number of identified INPs we were able to demonstrate that our method provides reliable and valid results for the main particle groups relevant to ice nucleation by comparing our main results with other INP/IR measurements performed at the high-altitude research station JFJ.

~~*Comparison to IR measurements from CLACE / INUIT 2017*~~

~~Our results for INPs activated in the deposition nucleation and condensation freezing modes at -30°C can be compared to IR measurements which were done during the same CLACE / INUIT 2017 campaign by other groups using Ice Counterflow Virtual Impactor (Ice-CVI; Mertes et al., 2007) as separation technique and different analyzing methods.~~

~~Eriksen Hammer et al. (2018) found similar particle classes as is presented here for their IRs collected between -10°C and -18°C and analyzed by SEM. Due to different activation conditions, freezing modes and sampling times, it is not possible to make detailed comparisons of the abundances of individual groups. For instance, soot is only activated as INP at very low temperatures, which explains the low abundances detected at - 30°C and its absence at warmer conditions as observed by Eriksen Hammer et al. (2018). Additionally, they sampled the total aerosol to investigate the enrichment or depletion of individual substances. In contrast to the composition of IRs, the total aerosol was primarily composed of complex secondary particles. As previously mentioned, our method is unable to detect these partially volatile compounds. However, their absence does not appear to significantly impact ice nucleation within the analyzed temperature range, thus not affecting the validity of our method.~~

~~Lacher et al. (2021) characterized IRs using the Aircraft-based laser ablation aerosol mass spectrometer (ALABAMA; Brands et al., 2011)). Consistent with our results and those by Eriksen Hammer et al. (2018), the dominant fraction was mineral dust (Al-rich + mineral dust) with a 58% abundance. Many mineral dust particles showed signals of biological material, which may be equivalent to the INPs in our study that exhibited a mixture of mineral and carbonaceous components. The lower percentage of mixed mineral particles in our case may be due to colder activation temperatures during the FRIDGE measurement, where activation of pure minerals is more likely. Metals, biological particles, and elemental carbon were also found in a similar percentage as in our distribution. However, since the classification of the particles followed a different scheme, the remaining groups cannot be directly compared.~~

~~*Comparison to INP/IR measurements from previous studies at the high- altitude research station JFJ*~~

~~The chemical composition of INPs presented here is in good agreement with previous studies conducted at the high-altitude research station JFJ. However, due to the use of different methods, only a rough comparison can be made among the main particle classes.~~

~~Mineral components have already been identified by earlier studies as an important feature of IRs at JFJ. Kamphus et al. (2010) reported a significant enrichment of mineral dust in IRs compared to the total aerosol (57 % compared to 17 %), using Ice-CVI and mass spectrometry. Worringen et al. (2015) also found terrigenous material as the main component in their INPs and IRs analyzed by SEM. Depending on the sampling technique, the values were ranging from 32% to 55%. The magnitude of both results agrees well with our mineral dust proportions in INPs.~~

~~Carbonaceous material was also identified as INPs / IRs at JFJ during winter 2013 by Worringen et al. (2015). The relative number abundances for these particles are in good agreement with our measurements for two of the three sampling methods they used (Ice-CVI, Ice Selective Inlet (ISI) and Fast Ice Nucleus Chamber (FINCH) + Ice Nuclei Pumped Counterflow Virtual Impactor (IN-PCVI)). The authors suggest that the higher proportion of carbonaceous particles observed with ISI is likely due to the collection of different air masses at the end of the campaign.~~

~~Metallic particles and metal oxides have also been identified as ice-forming compounds in previous studies conducted at JFJ. Kamphus et al. (2010) reported the presence of 14 % metallic particles in their IRs, but their classification scheme is not directly comparable to ours. Ebert et al. (2011) collected IRs by Ice-CVI separation to study them with EM. They also found metal oxides in their IRs and classified them primarily as iron oxide, which is consistent with our results. Worringen et al. (2015) also reported the existence of metal oxides in IRs and INPs, with relative number abundances ranging from 5% to 20 %. Our calculated fraction of 4 % agrees well with their lower limit.~~

~~A clear enrichment of complex mixtures in the IRs compared to the total aerosol was found by Ebert et al. (2011). Half of the particles in this group were described as silicate mixture particles that mainly contained carbonaceous material as well. This corresponds to our mixed group. Such a silicate mixture group was also defined by Worringen et al. (2015), in relative proportions corresponding to what we have found.~~

3.~~4~~5 Chemically-resolved INP size distribution

In addition to providing information on the concentration and chemical ~~classification~~ composition of INPs, our coupling method ~~also yields~~ offers ~~data on their size. This is a~~the significant advantage ~~in~~ of~~creating~~ providing an INP size distribution that can be coupled to the chemistry of individual INPs.~~, as it offers information about the chemical composition of each individual size bin.~~The size of each identified INP is determined by calculating the projected area diameter (d_{pa}).

Figure 10~~7~~ shows the chemically~~-~~-resolved size distribution of all identified INPs from the CLACE~~-/-~~INUIT 2017 campaign at the high-altitude research station JFJ. The graph displays the absolute INP numbers within a specific size range (blue line), with the maximum found between 1 µm and 2 µm. All particles with d_{pa} > 6 µm were summarized due to statistical purposes. In comparison to the ~~a~~ total aerosol size distribution from the ~~FT at JFJ (e.g., Nyeki et al., 1998)~~ whole campaign period (Weber, 2019), the maximum of the INP size distribution is significantly shifted towards larger diameters. We

hypothesize that, in addition to the primary suitability of larger particles as ice nuclei, the ~~volatility~~ absence of the small volatile aerosol components (nitrates, sulfates, and volatile organics) may play a role here (see Sect. 2.6). ~~As mentioned above, these volatile compounds cannot be detected by our coupling technique, which is why this method is limited to the analysis of non-volatile substances.~~In an enrichment and depletion study, Eriksen Hammer et al. (2018) determined the depletion of the complex secondary aerosol in IRs compared to the total aerosol. This leads to the conclusion that the absence of these compounds does not significantly influence the results.

hat formatiert: Schriftfarbe: Automatisch

hat formatiert: Schriftfarbe: Automatisch

hat formatiert: Schriftfarbe: Automatisch

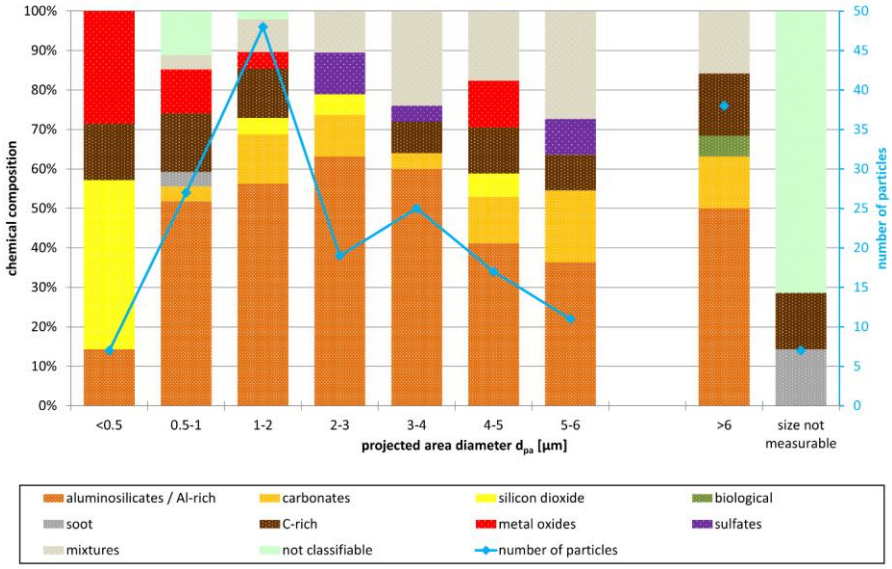

Figure 10~~7~~: Chemically resolved size distribution for all identified INPs (artifact excluded; n = 199) from CLACE/INUIT 2017 at the high-altitude research station Jungfraujoch (activated at T = -30 °C and RH = 99 / 101 %; RH = 95 / 97% was chosen for one sample due to cluster formation at higher RH~~RH = 95 / 97 / 99 / 101 %~~).

hat formatiert: Schriftart: Fett

As the mineral particles (aluminosilicates / Al-rich, carbonates and silicon dioxide) are in general the most prevalent group within the analyzed samples, they are also the most prevalent group in all size ranges, with proportions ranging from 50 % to ~~100~~80 %. The proportions of the individual components vary for the different size ranges. However, the aluminosilicates / Al-rich particles represent the most abundant group among all size bins from d_{pa} > 0.5 µm.

Only 3 % of the analyzed INPs had a quantifiable diameter smaller than 0.5 µm. The smallest INP whose size could be determined with confidence was 300 nm, although we can generally also see smaller particles in the SEM. This agrees to

well-established findings in the literature substantiating that most particles ~~only~~ that act as effective ice nuclei are above a size of 500 nm (DeMott et al., 2010). Besides the mineral particles, which primarily consist of silicon dioxide ~~(both spherical and non-spherical)~~, the smallest size bin shows the highest proportion of metal oxides ~~(non-spherical)~~.

Significantly more particles (14 % ~~of all identified INPs~~) were found in the size range between 0.5 µm and 1 µm. ~~The mineral fraction is manly composed of aluminosilicates / Al-rich particles, with a small number of carbonates.~~ In addition to the mineral fraction, ~~Additionally, soot and C-rich~~carbonaceous particles as well as metal oxides and mixtures can be assigned to this ~~second~~ size bin. However, due to their submicron size, some particles could not be chemically classified.

The size range of 1-2 µm contained the largest number of INPs (24 % ~~in total~~), with a similar chemical composition to the previous size bin. ~~Again, aluminosilicates / Al-rich particles are the most abundant group in the mineral fraction. Additional contributions from carbon containing particles, metal oxides and mixtures are reported.~~

The number of particles decreases for INPs with d_{pa} > 2 µm, which is consistent with a lower occurrence of these particles due to a reduced residence time in the free troposphere. ~~as particle size increases. Besides the mineral fraction, which is mainly represented by Aluminosilicates / Al-rich particles and carbonates, t~~The proportion of mixtures increases notably for INPs larger 2 µm. Additionally, C-rich particles ~~All sulfates~~were ~~can also be~~ found in ~~this~~the range . ~~C-rich particles are also found to be distributed over the entire size range~~ up to ~~6~~10 µm, as well as all sulfates. ~~All sulfates can also be found in this range.~~

Since the abundance of INPs with d_{pa} > ~~6~~10 µm is low ~~(8 %)~~ in the individual size ranges, they are summed up. The largest INP had a d_{pa} of 34.5 µm. ~~Besides~~ Apart from mineral particles, ~~and~~ C-rich particles, and mixtures, the two biological particles were also found in this size range. Due to losses by sedimentation, long-range transport of ~~these~~ large particles is very unlikely. However, a local influence by air that is advected from the planetary boundary layer to the station cannot be excluded. ~~Besides mineral particles and C-rich particles, the two biological particles were also found in this size range.~~

It was not possible to determine the size of some particles, as their small size caused them to provide an insufficient image. ~~No d_{pa} could be determined for~~This was the case for some carbonaceous particles ~~C-rich and soot particles,~~ as well as for ~~most~~ those particles for which ~~without~~ a chemical classification was also not possible ~~, since they were mostly too small to get a usable image~~.

~~Note the relatively high statistical uncertainty due to the low INP numbers.~~

Lacher et al. (2021) and Worringen et al. (2015) provide size distributions for INPs/IRs measured with different techniques at the high-altitude research station JFJ up to a size of 3 µm and 5 µm, respectively. In both studies, the highest concentration was found for IRs smaller than 0.5 µm, but ~~measured the size distribution of IRs during CLACE / INUIT 2017 downstream of an Ice-CVI using an optical particle counter with a size range of 0.3-5 µm. The highest concentration was found for IRs with a diameter of 0.3 µm. The~~ the ~~secondary~~ broad maximum ~~with~~ (diameters between 1.3 µm and 5 µm) from Lacher et al. (2021) agrees reasonably well to our findings. ~~Comparing the chemically resolved size distribution of IRs analyzed with~~

~~ALABAMA to what is presented here is difficult because the majority of IRs analyzed by Lacher et al. (2021) were smaller than 1 µm.~~

~~Worringen et al. (2015) also determined size distributions (maximum particle size 3 µm) for their major INP/IR components. In each of their three different sampling setups, the maximum particle number was found to be between 0.3 and 0.5 µm diameter.~~ The ~~same~~ is the case for particles collected with the Ice Selective Inlet~~SI~~ by Worringen et al. (2015), which also showed a second~~ary~~ maximum at 1 - 1.5 µm~~, which is the same range as our maximum~~. The shift towards larger particle diameters in our results in comparison to the maxima from Lacher et al. (2021) and Worringen et al. (2015) may be caused by the differences in sampling and ice activation. ~~When collecting IRs using any type of counterflow virtual impactor, there is always a size selection of the ice crystals, which indirectly affects the resulting INP/IR size distribution.~~ INPs in FRIDGE are activated through deposition nucleation / condensation freezing under defined conditions, while the IRs collected from ambient air are activated under natural and even more complex conditions, including the potentially more important immersion freezing mode (~~Lohmann et al., 2016~~Ansmann et al., 2009; Murray et al., 2012).

The comparison of such INP size distributions with chemical information from different methods is difficult, since in addition to the influencing factors discussed in Sect. 3.3, a possible size selection or limitation of the sampling process, and different techniques of particle sizing may also play a role. Nevertheless, the results for our main groups are in reasonable agreement with the results from Worringen et al. (2015). In our results, both the metal oxides and the few soot particles were observed at very small diameters, which is comparable to carbonaceous particles/soot and metal oxides predominantly detected in the submicron range by Worringen et al. (2015). Terrigenous particles, including silicates and Ca-rich particles, were primarily found in the larger size ranges, while our ~~carbonaceous particles/soot and metal oxides were predominantly detected in the submicron range. In our results, both the metal oxides and the few soot particles also showed very small diameters, while the~~ mineral components were distributed over all size ranges, with silicates domination for particles from d_{pa} > 0.5 µm. In contrast to Worringen et al. (2015), our C-rich particles were present over the entire size range. The reason for this is possibly that our classification scheme assigned the larger potentially biological particles as C-rich.

~~The shift towards larger particle diameters in our results in comparison to the maxima from Lacher et al. (2021) and Worringen et al. (2015) may be caused by the differences in sampling and ice activation. When collecting IRs using any type of counterflow virtual impactor, there is always a size selection of the ice crystals, which indirectly affects the resulting INP/IR size distribution. INPs in FRIDGE are activated through deposition nucleation / condensation freezing under defined conditions, while the IRs collected from ambient air are activated under natural and even more complex conditions, including the potentially more important immersion freezing mode (Lohmann et al., 2016).~~

4 Summary and conclusions

A method for analyzing the concentration and individual physico-chemical properties of ambient INPs, which has been used in several campaigns (Schrod et al., 2020b; He et al., 2023), is discussed here from a methodological perspective. has been developed. The method benefits from the coupling of two instruments already used for the analysis of INPs and IRs: the static diffusion chamber FRIDGE and the SEM. As the individual methods are already known, the focus here was on a description of the coupling and the associated advantages and uncertainties, as well as the resulting potential of the method. This coupling allows for detailed analysis of various INP properties, such as chemical composition, mixing state, size, morphology, and surface properties like cracks or pores.

In this study aAmbient atmospheric aerosol samples were are collected onto silicon wafer substrates using a simple electrostatic precipitator setup. Deposition nucleation and condensation freezing mode INPs were are activated in the static diffusion chamber FRIDGE at various combinations of temperature and humidity and the resulting ice crystal growth is photographed in the static diffusion chamber FRIDGE at several combinations of temperature and humidity. The ice crystal center points are located using an image analysis software based on the pictures taken during the FRIDGE measurement. Engraved calibration marks were used to transfer the center point coordinates of the ice crystals grown in the FRIDGE experiment to the electron microscope. It washas been shown, that this position calculation works reasonably well, with a neglectablenegligible number of misplaced incorrect positions. Engraved calibration marks were are used to transfer the calculated ice crystal center point coordinates of the ice crystals grown in the FRIDGE experiment to the electron microscope. Uncertainties for the center point calculation and the calibration were discussed, with the conclusion that it is necessary to consider not only the exact coordinate but also the surrounding area. Considering the uncertainties and the desired low probability of observing multiple particles within the scan area, a scan radius of 50 µm around the calculated coordinate was established as a guideline. This limitation may lead to the exclusion of potential INPs in the case of particle drift, miscalculated ice crystal origins or more than one particle present in the scanned area. At the same time, it increases the accuracy of the results, because we are analyzing only those particles which can be unambiguously associated with the origin of a real grown ice crystal. The identification rate has been calculated to be 30 % for the presented field data, but may vary for other samples as it strongly depends on the total wafer loading. Comprehensive single particle analysis Observing every single ice crystal origin using aby SEM with and EDX detector provided the opportunity to comprehensively analyze the properties of individual INPs at each position where only one particle was is found in the defined radius around the coordinate, provides the chemical composition of the associated INP, as well as information on its size and morphology. . A size distribution of the number and composition of INPs can be achieved. The identification rate was calculated at 30 % for the presented field data, but may vary for other samples, as it depends strongly on the total wafer loading.

Although the method has some drawbacks and uncertainties, it enables high accuracy in the identification of ice-active particles. This is, from our point of view, its significant strength compared to other INP/IR methods, which may have difficulties distinguishing between true INPs/IRs, additional collected particles, and sampling artifacts. In addition, this

method can also determine ice activity for particles with a size of several micrometers, making it a useful complement to methods with size restrictions due to inlet systems or other factors. The detailed information on physico-chemical particle properties that can be obtained from SEM can be a valuable addition to pure INP counting methods for gaining information on the relevance of particle properties to ice nucleation efficiencies and could help to bridge the knowledge gap towards INP aerosol-type-specific parametrizations that could be used in modeling studies (Burrows et al., 2022).

The presented case study with samples from the CLACE/INUIT 2017 campaign at the high-altitude research station JFJ demonstrates that the method yields valuable results for the main INP classes, despite comparably low counting statistics. However, detailed statements about the minor INP classes are not possible for this study. Mineral components (aluminosilicates / Al-rich particles, carbonates and silicon dioxide), were the most prevalent as INPs in the predominantly free tropospheric air masses at the JFJ. They were distributed over the entire size range, except for silicon dioxide, which was mainly found in the size range below 500 nm. These particles originated mainly from non-local background dust sources - and in particular from a SDE, which can also be identified by a different chemical INP composition. Carbonaceous INPs of various sizes were found, including a minute amount of small soot particles as well as large biological particles. In addition, a small amount of metal oxides, mostly iron oxide, were also identified, primarily with $d_{ps} < 0.5$ µm. Sulfates were rare. Mixed particles, predominantly aluminosilicate / Al-rich particles with increased carbon content, were more common at larger diameters with a higher proportion in air masses prior to the SDE.

Future studies may relate the composition and sizes of INPs to the different activation conditions. ~~By using position data sets from different sets of activation conditions, future studies may relate the composition and sizes of INPs to the different activation conditions.~~ This may help to identify which particle types and features are atmospherically most relevant as a function of temperature. ~~However, due to the relatively low counting statistics, further improvements are necessary to obtain a more reliable insight into the relevance of the particle properties for the INP activation.~~ The comprehensive single particle information provides also the opportunity to study for example the potential enrichment of high-effective ice nucleating particles (e.g., K-rich feldspar) by comparing the activated particles to the total wafer loading. However, due to the relatively low counting statistics, further improvements are necessary to obtain a more reliable insight into the relevance of the particle properties for the INP activation.

~~The presented analysis of INPs collected at the high-altitude research station JFJ in winter 2017 demonstrates the benefits of coupling FRIDGE to the SEM. The results are generally comparable to ones from other methods, partially obtained at the same location or even within the same campaign. However, the size distribution obtained by this technique differs from others, which may be related to the sampling mechanism and activation conditions.~~

~~The mineral components, mainly aluminosilicates / Al-rich particles, but also carbonates and silica, were clearly dominant as INPs in the predominantly free tropospheric air masses at the JFJ. They were distributed over the entire size range, except for silicon dioxide, which was mainly found in the size range below 500 nm. These components originated primarily from non-local background dust sources - and specifically from a Saharan dust event. They were distributed over the entire size range, except for silicon dioxide, which was mainly found in the size range below 500 nm. We found carbonaceous INPs of various sizes, including a minute amount of small soot particles as well as large biological particles. Additionally, a small amount of metal oxides, mostly iron oxide, with primarily d_{pa} < 500 µm were also identified. Sulfates were rare. Mixed particles, predominantly aluminosilicate / Al-rich particles with increased carbon content, were more frequently found at larger diameters.~~

~~The results from several campaigns (Schrod et al., 2017; Schrod et al., 2020b; Weber, 2019; He et al., 2023) consistently demonstrate the potential of coupling the two instruments for the detailed analysis of deposition nucleation / condensation freezing mode INPs. This method can also determine ice activity for particles with a size of several micrometers, making it a useful complement to methods with size restrictions due to inlet systems or other factors. Together with the structural information that can be obtained from SEM, it can be a valuable addition to pure INP counting methods for gaining information on the relevance of particle properties to ice nucleation efficiencies. The resulting information about the physico-chemical properties of individual INPs could help to bridge the knowledge gap towards INP aerosol type specific parametrizations that could be used in modeling studies.~~

As experimental knowledge about concentration and composition of INPs, and their contribution to upper tropospheric ice nucleation processes in cirrus cloud formation is severely lacking (Kanji et al., 2017), the method will be adapted for future aircraft campaigns.

Data availability

The complete data set is available for the community and can be accessed by request to ~~Lisa Schneider (schneider@geo.tu-darmstadt.de) or~~ Martin Ebert (mebert@geo.tu-darmstadt.de) of the Technical University Darmstadt.

Author contributions

The concept of the study was designed by JC, ME and HB. The samples at the high-altitude research station Jungfraujoch were collected by DW, who also performed the FRIDGE measurements and interpreted the INP concentration data with HB, JC and JS. The scanning electron microscopy analysis was performed by LS, the interpretation was done with support from ME. KK wrote the program to perform the ice crystal center determination and coordinate conversion. The general method evaluation was done by LS, KK, HB, JS, ME. The paper concept was drafted and written by LS ~~and JS~~, with contributions from JS, DW, HB, JC, ME and KK.

Competing interests

One Co-author is member of the editorial board of the journal Atmospheric Measurement Techniques.

Acknowledgements

This work was funded by the Deutsche Forschungsgemeinschaft (DFG, German Research Foundation) – TRR 301 – Project-ID 428312742 and by the Ice nucleating research unit INUIT (FOR 1525 (project ID 170852269)).

References

~~Abdelmonem, A., Ratnayake, S., Toner, J. D., Lützenkirchen, J.: Cloud history can change water ice surface interactions of oxide mineral aerosols: a case study on silica, Atmos. Chem. Phys., 20, 1075-1087, doi:10.5194/acp-20-1075-2020, 2020~~

Ansmann, A., Bösenberg, J., Chaikovsky, A., Comerón, A., Eckhardt, S., Eixmann, R., Freudenthaler, V., Ginoux, P., Komguem, L., Linné, H., López Marquez, M. Á., Matthias, V., Mattis, I., Mitev, V., Müller, D., Music, S., Nickovic, S., Pelon, J., Sauvage, L., Sobolewsky, P., Srivastava, M. K., Stohl, A., Torres, O., Vaughan, G., Wandinger, U., Wiegner, M.: Long-range transport of Saharan dust to norther Europe: The 11-16 October 2001 outbreak observed with EARLINET, J. Geophys. Res., 108, 4783, doi: 10.1029/1003JD003757, 2003

Ansmann, A., Tesche, M., Seifert, P., Althausen, D., Engelmann, R., Fruntke, J., Wandinger, U., Mattis, I., Müller, D.: Evolution of ice phase in tropical altocumulus: SAMUM lidar observations over Cape Verde, J. Geophys. Res., 114, D17208, doi: 10.1029/2008JD011659, 2009

Archuleta C. M., DeMott, P. J., Kreidenweis, S. M.: Ice nucleation by surrogates for atmospheric mineral dust and mineral dust/sulfate particles at cirrus temperatures, Atmos. Chem. Phys., 5, 2617-2634, doi: 10.5194/acp-5-2617-2005, 2005

Baltensperger, U., Schwikowski, M., Jost, D. T., Nyeki, S., Gäggeler, H. W., Poulida, O.: Scavenging of atmospheric constituents in mixed phase clouds at the high-alpine site Jungfraujoch Part I: Basic concept and aerosol scavenging by clouds, Atmos. Environ., Vol. 32, No. 23, 3975-3983, 1998

Boose, Y., Welti, A., Atkinson, J., Ramelli, F., Danielczok, A., Bingemer, H. G., Plötze, M., Sierau, B., Kanji, Z. A., Lohmann, U.: Heterogeneous ice nucleation on dust particles sourced from nine deserts worldwide – Part 1: Immersion freezing, Atmos. Chem. Phys., 16, 15075-15095, doi: 10.5194/acp-16-15075-2016, 2016

hat formatiert: Englisch (Vereinigte Staaten)

hat formatiert: Englisch (Vereinigte Staaten)

hat formatiert: Englisch (Vereinigte Staaten)

hat formatiert: Englisch (Vereinigte Staaten)

Brands, M., Kamphus, M., Böttger, T., Schneider, J., Drewnick, F., Roth, A., Curtius, J. Voigt, C., Borbon, A., Beekmann, M., Bourdon, A., Perrin, T., Borrmann, S.: Characterization of a Newly Developed Aircraft-Based Laser Ablation Aerosol Mass Spectrometer (ALABAMA) and First Field Deployment in Urban Pollution Plumes over Paris During MEGAPOLI 2009, Aerosol Sci. Tech., 45:1, 46-64, doi: 10.1080/02786826.2010.517813, 2011

Brasseur, Z., Castarède, D., Thomson, E. S., Adams, M. P., Drossaart van Dusseldorp, S., Heikkilä, P., Korhonen, K., Lampilahti, J., Paramonov, M., Schneider, J., Vogel, F., Wu, Y., Abbatt, J. P. D., Atanasova, N. S., Bamford, D. H., Bertozzi, B., Boyer, M., Brus, D., Daily, M. I., Fösig, R., Gute, E., Harrison, A. D., Hietala, P., Höhler, K., Kanji, Z. A., Keskinen, J., Lacher, L., Lampimäki, M., Levula, J., Manninen, A., Nadolny, J., Peltola, M., Porter, G. C. E., Poutanen, P., Proske, U., Schorr, T., Umo, N. S., Stenszky, J., Virtanen, A., Moisseev, D., Kulmala, M., Murray, B. J., Petäjä, T., Möhler, O., Duplissy, J.: Measurement report: Introduction to the HyICE-2018 campaign for measurements of ice-nucleating particles and instrument inter-comparison in the Hyytiälä boreal forest, Atmos. Chem. Phys., 22, 5117-5145, doi: 10.5194/acp-22-5117-2022, 2022

Bukowiecki, N., Weingartner, E., Gysel, M., Collaud Coen, M, Zieger, P., Herrmann, E., Steinbacher, M., Gäggeler H. W., Baltensperger U.: A Review of More than 20 Years of Aerosol Observation at the High-Altitude Research Station Jungfraujoch, Switzerland (3580 m asl), Aerosol Air Qual. Res., 16, 764-788, doi: 10.4209/aaqr.2015.05.0305, 2016

Bundke, U., Nillius, B., Jaenicke, R., Wetter, T., Klein, H., Bingemer, H.: The fast Ice Nucleus chamber FINCH, Atmos. Res., 90, 180-186, doi: 10.1016/j.atmosres.2008.02.008, 2008

Burrows, S. M., McCluskey, C. S., Cornwell, G., Steinke, I., Zhang, K., Zhao, B., Zawadowicz, M., Raman, A., Kulkarni, G., China, S., Zelenyuk, A., DeMott, P. J.: Ice-Nucleating Particles That Impact Clouds and Climate: Observational and Modeling Research Needs, Rev. Geophys., 60, doi: 10.1029/2021RG000745, 2022

Cozic, J., Mertes, S., Verheggen, B., Cziczo, D. J., Gallavardin, S. J., Walter, S., Baltensperger, U., Weingartner, E.: Black carbon enrichment in atmospheric ice particle residuals observed in lower tropospheric mixed phase clouds, J. Geophys. Res., 113, D15209, doi: 10.1029/2007JD009266, 2008

Cziczo, D. J., Stetzer, O., Worringen, A., Ebert, M., Weinbruch, S., Kamphus, M., Gallavardin, S. J., Curtius, J., Borrmann, S. Froyd, K. D., Mertes, S., Möhler, O., Lohmann, U.: Inadvertent climate modification due to anthropogenic lead, Nat. Geosci., 2, 333-336, doi: 10.1038/ngeo499, 2009

hat formatiert: Deutsch (Deutschland)

hat formatiert: Englisch (Vereinigte Staaten)

Cziczo, D. J., Froyd, K. D., Hoose, C., Jensen, E. J., Diao, M., Zondlo, M. A., Smith, J. B., Twohy, C. H., Murphy, D. M.: Clarifying the Dominant Sources and Mechanisms of Cirrus Cloud Formation, Science, Vol. 340, 1320 – 1324, doi: 10.1126/science.1234145, 2013

Cziczo, D. J., Ladino, L., Boose, Y., Kanji, Z. A., Kupiszewski, P., Lance, S., Mertes, S., Wex, H.: Measurements of Ice Nucleating Particles and Ice Residuals, Meteor. Mon., 58, 1-13, doi: 10.1175/AMSMONOGRAPHS-D-16-0008.1, 2017

DeMott, P. J., Prenni, A. J., Liu, X., Kreidenweis, S. M., Petters, M. D., Twohy, C. H., Richardson, M. S., Eidhammer, T., Rogers, D. C.: Predicting global atmospheric ice nuclei distributions and their impacts on climate, P. Natl. A. Sci, 107, no. 25, 11217-11222, doi: 10.1073/pnas.0910818107, 2010

DeMott, P. J., Möhler, O., Cziczo, D., Hiranuma, N., Petters, M. D., Petters, S. S., Belosi, F., Bingemer, H. G., Brooks, S. D., Budke, C., Burkert-Kohn, M., Collier, K. N., Danielczok, A., Eppers, O., Felgitsch, L., Garimella, S., Grothe, H., Herenz, P., Hill, T. C. J., Höhler, K., Kanji, Z. A., Kiselev, A., Koop, T., Kristensen, T. B., Krüger, K., Kulkarni, G., Levin, E. J. T., Murray, B. J., Nicosia, A., O'Sullivan, D., Peckhaus, A., Polen, M. J., Price, H. C., Reicher, N., Rothenberg, D. A., Rudich, Y., Santachiara, G., Schiebel, T., Schrod, J., Seifreid, T. M., Stratmann, F., Sullivan, R. C., Suski, K. J., Szakáll, M., Taylor, H. P., Ullrich, R., Vergara-Temprado, J., Wagner, R., Whale, T. F., Weber, D., Welti, A., Wilson, T. W., Wolf, M. J., Zenker, J.: The Fifth International Workshop on Ice Nucleation phase 2 (FIN-02): laboratory intercomparison of ice nucleation measurements, Atmos. Meas. Tech., 11, 6231-6257, doi: 10.5194/amt-11-6231-2018, 2018

DeMott, P. J., Mirrielees, J. A., Petters, S., S., Cziczo, D. J., Petters, M. D., Bingemer, H. G., Hill, T. C. J., Froyd, K., Garimella, S., Hallar, A. G., Levin, E. J. T., McCubbin, I. B., Perring, A. E., Rapp, C. N., Schiebel, T., Schrod, J., Suski, K. J., Weber, D., Wolf, M. J., Zawadowicz, M., Zenker, J., Möhler, O., Brooks, S. D.: The Fifth International Workshop on Ice Nucleation Phase 3 (FIN-03): Field Intercomparison of Ice Nucleation Measurements, EGUsphere [preprint], doi: 10.5194/egusphere-2024-1744, 21 June 2024

Després, V. R., Huffman, J. A., Burrows, S. M., Hoose, C., Safatov A. S., Buryak G., Fröhlich-Nowoisky, J., Elbert, W., Andreae, M. O., Pöschl, U., Jaenicke, R.: Primary biological aerosol particles in the atmosphere: a review, Tellus B, 64:1, doi: 10.3402/tellusb.v64i0.15598, 2012

Ebert, M., Weinbruch, S., Hoffmann, P., Ortner, H. M.: Chemical characterization of North Sea aerosol particles, J. Aerosol Sci., Vol. 31, No. 5, 613-632, 2000

Ebert, M., Worringen, A., Benker, N., Mertes, S., Weingartner, E., Weinbruch, S.: Chemical composition and mixing-state of ice residuals sampled within mixed phase clouds, Atmos. Chem. Phys., 11, 2805-2816, doi: 10.5194/acp-11-2805-2011, 2011

Eriksen Hammer, S., Mertes, S., Schneider, J., Ebert, M., Kandler, K., Weinbruch, S.: Composition of ice particle residuals in mixed-phase clouds at Jungfraujoch (Switzerland): enrichment and depletion of particle groups relative to total aerosol, Atmos. Chem. Phys., 18, 1387-1403, doi: 10.5194/acp-18-13987-2018, 2018

Eriksen Hammer, S., Ebert, M., Weinbruch, S.: Comparison of operator- and computer-controlled scanning electron microscopy of particles from different atmospheric aerosol types, Anal. Bioanal. Chem., 411:1633-1645, doi: 10.1007/s00216-019-01614-7, 2019

He, C., Yin, Y., Huang, Y., Kuang, X., Cui, Y., Chen, K., Jiang, H., Kiselev, A., Möhler, O., Schrod, J.: The Vertical Distribution of Ice-Nucleating Particles over the North China Plain: A Case of Cold Front Passage, Remote Sens., 15, 4989, doi: 10.3390/rs15204989, 2023

Herrmann, E., Weingartner, E., Henne, S., Vuilleumier, L., Bukowiecki, N., Steinbacher, M., Conen, F., Collaud Coen, M., Hammer, E., Jurányi, Z., Baltensperger, U., Gysel, M.: Analysis of long-term aerosol size distribution data from Jungfraujoch with emphasis on free tropospheric conditions, cloud influence, and air mass transport, J. Geophys. Res.-Atmos., 9459 – 9480, doi: 10.1002/201JD023660, 2015

Hiranuma, N., Augustin-Bauditz, S., Bingemer, H., Budke, C., Curtius, J., Danielczok, A., Diehl, K., Dreischmeier, K., Ebert, M., Frank, F., Hoffmann, N., Kandler, K., Kiselev, A., Koop, T., Leisner, T., Möhler, O., Nillius, B., Peckhaus, A., Rose, D., Weinbruch, S., Wex, H., Boose, Y., DeMott, P. J., Hader, J. D., Hill, T. C. J., Kanji, Z. A., Kulkarni, G., Levin, E. J. T., McCluskey, C. S., Murakami, M., Murray, B. J., Niedermeier, D., Petters, M. D., O'Sullivan D., Saito, A., Schill, G. P., Tajiri, T., Tolbert, M. A., Welti, A., Whale, T. F., Wright T. P., Yamashita, K.: A comprehensive laboratory study on the immersion freezing behavior of illite NX particles: a comparison of 17 ice nucleation measurement techniques, Atmos. Chem. Phys., 15, 2489-2518, doi: 10.5194/acp-15-2489-2015, 2015

Hiranuma, N., Adachi, K., Bell, D. M., Belosi, F., Beydoun, H., Bhaduri, B., Bingemer, H., Budke, C., Clemen, H.-C., Conen, F., Cory, K. M., Curtius, J., DeMott, P. J., Eppers, O., Grawe, S., Hartmann, S., Hoffmann, N., Höhler, K., Jantsch, E., Kiselev, A., Koop, T., Kulkarni, G., Mayer, A., Murakami, M., Murray, B. J., Nicosia, A., Petters, M. D., Piazza, M., Polen, M., Reicher, N., Rudich, Y., Saito, A., Santachiara, G., Schiebel, T., SChill, G. P., Schneider, J., Segev, L., Stopelli, E:, Sullivan, R. C., Suski, K., Szakáll, M., Tajiri, Z., Taylor, H., Tobo, Y., Ullrich, R., Weber, D.,

Wex, H., Whale, T. F., Whiteside, C. L., Yamashita, K., Zelenyuk, A., Möhler, O.: A comprehensive characterization of ice nucleation by three different types of cellulose particles immersed in water, Atmos. Chem. Phys., 19, 4823-4849, doi: 10.5194/acp-19-4823-2019, 2019

Hoose, C. and Möhler, O.: Heterogeneous ice nucleation on atmospheric aerosols: a review of results from laboratory experiments, Atmos. Chem. Phys., 12, 9817-9854, doi: 10.5194/acp-12-9817-2012, 2012

Jing, X., Yang, J., Li, T., Hu, J., He, C., Yin, Y., DeMott, P. J., Wang, Z., Jiang, H., Chen, K.: Pre-Activation of Ice Nucleating Particles in Deposition Nucleation Mode: Evidence from Measurement Using a Static Vacuum Water Vapor Diffusion Chamber in Xinjiang, China, Geophys. Res. Lett., 49, e2022GL099468, doi: 10.1029/2022GL099468, 2022

Kamphus, M., Ettner-Mahl, M., Klimach, T., Drewnick, F., Keller, L., Cziczo, D. J., Mertes, S., Borrmann, S., Curtius, J.: Chemical composition of ambient aerosol, ice residues and cloud droplet residues in mixed-phase clouds: single particle analysis during the Cloud and Aerosol Characterization Experiment (CLACE 6), Atmos. Chem. Phys., 10, 8077-8095, doi: 10.5194/acp-10-8077-2010, 2010

Kandler, K., Benker, N., Bundke, U., Cuevas, E., Ebert, M., Knippertz, P., Rodríguez, E., Schütz, L., Weinbruch, S.: Chemical composition and complex refractive index of Saharan Mineral Dust at Izaña, Tenerife (Spain) derived by electron microscopy, Atmos. Environ. 41, 8058-8074, doi: 10.1016/j.atmosenv.2007.06.047, 2007

Kanji, Z. A., Florea, O., Abbatt, J. P. D.: Ice formation via deposition nucleation on mineral dust and organics: dependence of onset relative humidity on total particulate surface area, Environ. Res. Lett., 3, 025004, doi: 10.1088/1748-9326/3/2/025004, 2008

Kanji, Z. A., Ladino, L. A., Wex, H., Boose, Y., Burkert-Kohn, M., Cziczo, D. J., Krämer, M.: Overview of Ice Nucleating Particles, Meteor. Mon., Vol. 58, doi: 10.1175/AMSMONOGRAPHS-D-16-0006.1, 2017

Kiselev, A., Bachmann, F., Pedevilla, P., Cox, S. J., Michaelides, A., Gerthsen, D., Leisner, T.: Active sites in heterogeneous ice nucleation – the example of K-rich feldspars, Science, 10, doi: 10.1126/science.aai8034, 2016

Klein, H., Haunold, W., Bundke, U., Nillius, B., Wetter, T., Schallenberg, S., Bingemer, H.: A new method for sampling of atmospheric ice nuclei with subsequent analysis in a static diffusion chamber, Atmos. Res., 96, 218-224, doi: 10.1016/j.atmores.2009.08.002, 2010

Kupiszewski, P., Weingartner, E., Vochezer, P., Schnaiter, M., Bigi, A., Gysel, M., Rosati, B., Toprak, E., Mertes, S., Baltensperger, U.: The Ice Selective Inlet. A novel technique for exclusive extraction of pristine ice crystals in mixed-phase clouds, Atmos. Meas. Tech., 8, 3087-3106, doi: 10.5194/amt-8-3087-2015, 2015

Kupiszewski, P., Zanatta, M., Mertes, S., Vochezer, P., Lloyd, G., Schneider, J., Schenk, L., Schnaiter, M., Baltensperger, U., Weingartner, E., Gysel, M.: Ice residual properties in mixed-phase clouds at the high-alpine Jungfraujoch site, J. Geophys. Res.-Atmos, 121, 12343-12362, doi: 10.1002/2016JD024894, 2016

Lacher, L., Clemen H.-C., Shen, X., Mertes, S., Gysel-Beer, M., Moallemi, A., Steinbacher, M., Henne, S., Saathoff, H., Möhler, O., Höhler, K., Schiebel, T., Weber, D., Schrod, J., Schneider, J., Kanji, Z. A.: Sources and nature of ice-nucleating particles in the free troposphere at Jungfraujoch in winter 2017, Atmos. Chem. Phys., 21, 16925-16953, doi: 10.5194/acp-21-16925-2021, 2021

Lacher, L., Adams, M. P., Barry, K., Bertozzi, B., Bingemer, H., Boffo, C., Bras, Y., Büttner, N., Castarede, D., Cziczo, D. J., DeMott, P. J., Fösig, R., Goodell, M., Höhler, K., Hill, T. C. J., Jentzsch, C., Ladino, L. A., Levin, E. J. T., Mertes, S., Möhler, O., Moore, K. A., Murray, B. J., Nadolny, J., Pfeuffer, T., Picard, D., Ramírez-Romero, C., Ribeiro, M., Richter, S., Schrod, J., Sellegri, K., Stratmann, F., Swanson, B. E., Thomson E. S., Wex, H., Wolf, M. J., Freney, E.: The Puy de Dôme ICe Nucleation Intercomparison Campaign (PICNIC): comparison between online and offline methods in ambient air, Atmos. Chem. Phys., 24, 2651-2678, doi: 10.5194/ACP-24-2651-2024, 2024

~~Lohmann, U., Lüönd, F., Mahrt, F.: An introduction to clouds, p. 229, Cambridge University Press, Cambridge, U.K., 381 pp., 2016~~Marcolli, C.; Pre-activation of aerosol particles by ice preserved in pores, Atmos. Chem. Phys., 17, 1595-1622, doi: 10.5194/acp-17-1595-2017, 2017

Mertes, S., Verheggen, B., Walter, S., Connolly, P., Ebert, M., Schneider, J., Bower, K. N., Cozic, J., Weinbruch, S., Baltensperger, U., Weingartner, E.: Counterflow Virtual Impactor Based Collection of Small Ice Particles in Mixed-Phase Clouds for the Physico-Chemical Characterization of Tropospheric Ice Nuclei: Sampler Description and First Case Study, Aerosol Sci. Tech., 41, 848-864, doi: 10.1080/02786820701501881, 2007

Murray, B. J., O'Sullivan, D., Atkinson, J. D., Webb, M. E.: Ice nucleation by particles immersed in supercooled cloud droplets, Chem. Soc. Rev., 41, 6519-6554, doi: 10.1039/c2cs35200a, 2012

Murray, B. J. and Liu, X.: Ice-nucleating particles and their effects on clouds and radiation, in: Aerosols and Climate, edited by Carslaw, K. S., Elsevier, 619-649, doi:10.1016/B978-0-12-819766-0.00014-6, 2022

Niemand, M., Möhler, O., Vogel, B., Vogel, H., Hoose, C., Connolly, P., Klein, H., Bingemer, H., DeMott, P., Skrotzki, J., Leisner, T.: A Particle-Surface-Area-Based Parametrization of Immersion Freezing on Desert Dust Particles, J. Atmos. Sci, 69 (10), 3077-3092, doi: 10.1175/JAS-D-11_0249.1, 2012

Nyeki, S., Li, F., Weingartner, E., Streit, N., Colbeck, I., Gäggeler, H. W., Baltensperger, U.: The background aerosol size distribution in the free troposphere: An analysis of the annual cycle at a high-alpine site, J. Geophys. Res., Vol. 103, D24, 31749-31761, doi: 10.1029/1998JD200029, 1998

Okada, K. and Kai, K.: Atmospheric mineral particles collected at Qira in the Taklamakan Desert, China, Atmos. Environ. 38, 6927-6935, doi: 10.1016/j.atmosenv.2004.03.078, 2004

O'Sullivan, D., Murray, B. J., Malkin, T. L., Whale, T. F., Umo, N. S., Atkinson, J. D., Price, H. C., Baustian, K. J., Browse, J., Webb, M. E.: Ice nucleation by fertile soil dusts: relative importance of mineral and biogenic components, Atmos. Chem. Phys., 14, 1853-1867, doi: 10.5194/acp-14-1853-2014, 2014

Perry, K. D., Cahill, T. A., Eldred, R. A., Dutcher, D. D.: Long-range transport of North African dust to the eastern United States, J. Geophys. Res., 102, 11,225-11,238, doi: 10.1029/97JD00260, 1997

Petters, M. D. and Wright, T. P.: Revisiting ice nucleation from precipitation samples, Geophys. Res. Lett., 42, 8758-8766, doi: 10.1002/2015GL065733, 2015

Pratt, K. A., DeMott, P. J., French, J. R., Wang, Z., Westphal, D. L., Heymsfield, A. J., Twohy, C. H., Prenni, A. J., Prather, K. A.: In situ detection of biological particles in cloud ice-crystals, Nat. Geosci., Vol. 2, 398 – 401, doi: 10.1038/NGEO521, 2009

Prenni, A. J., Petters, M. D., Kreidenweis, S. M., Heald, C. L., Martin, S. T., Artaxo, P., Garland, R. M., Wolly, A. G., Pöschl, U.: Relative roles of biogenic emissions and Saharan dust and ice nuclei in the Amazon basin, Nat. Geosci., Vol. 2, 402-405, doi: 10.1038/NGEO517, 2009

Pummer, B. G., Bauer, H., Bernardi, J., Bleicher, S., Grothe, H.: Suspendable macromolecules are responsible for ice nucleation activity of birch and conifer pollen, Atmos. Chem. Phys., 12, 2541-2550, doi: 10.5194/acp-12-2541-2012, 2012

hat formatiert: Englisch (Vereinigte Staaten)

hat formatiert: Englisch (Vereinigte Staaten)

Rogers, D. C.: Development of a Continuous Flow Thermal Gradient Diffusion Chamber for Ice Nucleation Studies, Atmos. Res., 22, 149-181, 1988

Schenk, L. P., Mertes, S., Kästner, U., Frank, F., Nillius, B., Bundke, U., Rose, D., Schmidt, S., Schneider, J., Worringen, A., Kandler, K., Bukowiecki, N., Ebert, M., Curtius, J., Stratmann, F.: Characterization and first results of an ice nucleating particle measurement system based on counterflow virtual impactor technique, Atmos. Meas. Tech. Discuss., 7, 10585-10617, doi: 10.5194/amtd-7-10585-2014, 2014

Schepanski, K.: Transport of Mineral Dust and Its Impact on Climate, Geosiences 2018, 8, 151, doi: 10.3390/geoscience8050151, 2018

Scheuvens, D. and Kandler, K.: On Composition, Morphology, and Size Distribution of Airborne Mineral Dust, in: Mineral Dust, edited by Knippertz, P. and Stuut, J.-B. W., Springer, Dordrecht, doi: 10.1007/978-94-017-8978-3_2, 2014

Schmidt, S., Schneider, J., Klimach, T., Mertes, S., Schenk, L. P., Kupiszewski, P., Curtius, J., Borrmann, S.: Online single particle analysis of ice particle residuals from mountain-top mixed-phase clouds using laboratory derived particle type assignment, Atmos. Chem. Phys., 17, 575-594, doi: 10.5194/acp-17-575-2017, 2017

Schneider, C. A., Rasband, W. S., Eliceiri, K. W., NIH Image to ImageJ: 25 years of image analysis, Nat. Methods, 9(7), 671-675, doi: 10.1038/nmeth.2089, 2012

Schrod, J., Danielczok, A., Weber, D., Ebert, M., Thomson E. S., Bingemer H. G.: Re-evaluating the Frankfurt isothermal static diffusion chamber for ice nucleation, Atmos. Meas. Tech., 9, 1313-1324, doi: 10.5194/amt-9-1313-2016, 2016

Schrod, J., Weber, D., Drücke, J., Keleshis, C., Pikridas, M., Ebert, M., Cvetkovic, B., Nickovic, S., Marinou, E., Baars, H., Ansmann, A., Vrekoussis, M., Mihalopoulos, N., Sciare, J., Curtius, J., Bingemer, H. G.: Ice nucleating particles over the Eastern Mediterranean measured by unmanned aircraft systems, Atmos. Chem. Phys., 17, 4817-4835, doi: 10.5194/acp-17-4817-2017, 2017

Schrod, J., Kleinhenz, D., Hörhold, M., Erhardt, T., Richter, S., Wilhelms F., Fischer, H., Ebert, M., Twarloh, B., Della Lunga, D., Jensen, C. M., Curtius, J., Bingemer, H. G.: Ice-nucleating particle concentrations of the past: insights from a 600-year-old Greenland ice core, Atmos. Chem. Phys., 20, 12459-12482, doi: 10.2194/acp-20-12459-2020, 2020a

Schrod, J., Thomson E. S., Weber, D., Kossmann, J., Pöhlker, C., Saturno J., Ditas, F., Artaxo, P., Clouard, V., Saurel, J.-M., Ebert, M., Curtius, J., Bingemer, H. G.: Long-term deposition and condensation ice-nucleating particle measurements from four stations across the globe, Atmos. Chem. Phys., 20, 15983 – 16006, doi: 10.5194/acp-20-15983-2020, 2020b

Schwarzenboeck, A., Heintzenberg, J., Mertes, S.: Incorporation of aerosol particles between 25 and 850 nm into cloud elements: measurments with a new complementary sampling system, Atmos. Res., 25, 241-260, doi: 10.1016/S0169-8059(99)00034-4, 2000

Sorensen, C. M., Feke, G. D.: The Morphology of Macroscopic Soot, Aerosol Sci. Tech., 25, 328-337, doi:10.1080/02786829608965399, 1996

Thomson, D. S., Schein, M. E., Murphy, D. M.: Particle Analysis by Laser Mass Spectrometry WB-57F Instrument Overview, Aerosol Sci. Tech., 33:153-169, doi: 10.1080/027868200410903, 2000

Vali, G., DeMott, P. J., Möhler, O., Whale, T. F.: Technical Note: A proposal for ice nucleation terminology, Atmos. Chem. Phys., 15, 10263 – 10270, doi: 10.5194/acp-15-10263-2015, 2015

Wilson, T. W., Ladino, L. A., Alpert, P. A., Breckels, M. N., Brooks, I. M., Browse, J., Burrows, S. M., Carslaw, K. S., Huffman, J. A., Judd, C., Kilthau, W. P., Mason, R. H., McFiggans, G., Miller, L. A., Nájera J. J., Polishchuk, E., Rae, S., Schiller, C. L., Si, M., Vergara Temprado, J., Whale, T. F., Wong, J. P. S., Wurl, O., Yakobi-Hancock, J. D., Abbatt, J. P. D., Aller, J. Y., Bertram, A. K., Knopf, D. A., Murray, B. J.: A marine biogenic source of atmospheric ice-nucleating particles, Nature 525, 234-238, doi: 10.1038/nature14986, 2015

Weber, D.: Eisnukleation von Aerosolen: Laborexperimente und Messungen im Feld, Ph.D. thesis, Goethe Universität Frankfurt, Germany, 2019

Welti, A., Lüönd, F., Stetzer, O., Lohmann, U.: Influence of particle size on the ice nucleating ability of mineral dusts, Atmos. Chem. Phys., 9, 6705-6715, doi: 10.5194/acp-9-6705-2009, 2009

Wex, H., Huang, L., Zhang, W., Hung, H., Traversi, R., Becagli, S., Sheesley, R. J., Moffett, C. E., Barrett, T. E., Bossi, R., Skov, H., Hünerbein, A., Lubitz, J., Löffler, M., Linke, O., Hartmann, M., Herenz, P., Stratmann, F.: Annual

hat formatiert: Englisch (Vereinigte Staaten)

hat formatiert: Englisch (Vereinigte Staaten)

hat formatiert: Englisch (Vereinigte Staaten)

hat formatiert: Englisch (Vereinigte Staaten)

hat formatiert: Englisch (Vereinigte Staaten)

hat formatiert: Englisch (Vereinigte Staaten)

hat formatiert: Englisch (Vereinigte Staaten)

variability of ice-nucleating particle concentrations at different Arctic locations, Atmos. Chem. Phys., 19, 5293-5311, doi: 10.5194/acp-19-5293-2019, 2019

Whalley, W. B. and Krinsley, D. H.: A scanning electron microscope study of surface textures of quartz grains from glacial environments, Sedimentology, 21, 87-105, doi:10.1111/j.1365-3091.1974.tb01783.x, 1974

Worringen, A., Kandler, K., Benker, N., Dirsch, T., Mertes, S., Schenk, L., Kästner, U., Frank, F., Nillius, B., Bundke, U., Rose, D., Curtius, J., Kupiszewski, P., Weingartner, E., Vochezer, P., Schneider, J., Schmidt, S. Weinbruch, S., Ebert, M.: Single-particle characterization of ice-nucleating particles and ice particle residuals sampled by three different techniques, Atmos. Chem. Phys., 15, 4161-4178, doi: 10.5194/acp-15-4161-2015, 2015

Yakobi-Hancock, J. D., Ladino, L. A., Abbatt, J. P. D.: Feldspar minerals as efficient deposition ice nuclei, Atmos.Chem. Phys., 13, 11175-11185, doi: 10.5194/acp-13-11175-2013, 2013